ÇUKUROVA UNIVERSITY
INSTITUTE OF NATURAL AND APPLIED SCIENCES

MSc THESIS

Murat DİLEK

MECHANICAL PROPERTIES OF DIFFERENT ALUMINUM ALLOYS JOINED BY FRICTION STIR WELDING

DEPARTMENT OF MECHANICAL ENGINEERING

ADANA, 2006

ÇUKUROVA ÜNİVERSİTESİ
FEN BİLİMLERİ ENSTİTÜSÜ

MECHANICAL PROPERTIES OF DIFFERENT ALUMINUM ALLOYS JOINED BY FRICTION STIR WELDING

Murat DİLEK

YÜKSEK LİSANS TEZİ

MAKİNA MÜHENDİSLİĞİ ANABİLİM DALI

Bu Tez 26/09/2006 Tarihinde Aşağıdaki Jüri Üyeleri Tarafından Oybirliği/Oyçokluğu ile Kabul Edilmiştir.

İmza:	İmza:	İmza:
Doç.Dr. Abdülkadir EKŞİ	Prof. Dr. Melih BAYRAMOĞLU	Doç.Dr. Cengiz D. ATİŞ
DANIŞMAN	ÜYE	ÜYE

Bu Tez Enstitümüz Makina Mühendisliği Anabilim Dalında Hazırlanmıştır.
Kod No:

Prof. Dr. Aziz ERTUNÇ
Enstitü Müdürü

Not: Bu tezde kullanılan özgün ve başka kaynaktan yapılan bildirişlerin, çizelge, şekil ve fotoğrafların kaynak gösterilmeden kullanımı, 5846 sayılı Fikir ve Sanat Eserleri Kanunundaki hükümlere tabidir.

ABSTRACT

M.Sc. THESIS

MECHANICAL PROPERTIES OF DIFFERENT ALUMINUM ALLOYS JOINED BY FRICTION STIR WELDING

MURAT DİLEK

DEPARTMENT OF MECHANICAL ENGINEERING
INSTITUTE OF NATURAL AND APPLIED SCIENCES
UNIVERSITY OF ÇUKUROVA

Supervisor: Assoc. Prof. Dr. Abdülkadir EKŞİ
Year: 2006, Pages: 74
Jury: Assoc. Prof. Dr. Abdülkadir EKŞİ
: Prof Dr. Melih BAYRAMOĞLU
: Assoc. Prof. Dr Cengiz D. ATİŞ

In this study, 5186-H111, 5083-O and 5083-H111 (Alustar) aluminum alloy plates were welded as similar and dissimilar alloy joints using Friction Stir Welding (FSW) process in order to investigate mechanical and microstructural properties. In order to investigate the effect of welding speeds on mechanical properties, metallographic and mechanical tests were carried out on the welded areas of the parts. Vickers hardness profile and tensile tests of the joints experimentally assessed. As a metallurgical investigation, Optic Microscopy and Scanning Electron Microscopy (SEM) were used for base and weld zones.

Keywords: Friction Stir Welding, Welding of Al Alloys, 5186-H111, 5083-O, 5083-H111 (Alustar)

ÖZ

YÜKSEK LİSANS TEZİ

SÜRTÜNME KARIŞTIRMA KAYNAĞI İLE BİRLEŞTİRİLEN
FARKLI ALUMİNYUM ALAŞIMLARININ
MEKANİK ÖZELLİKLERİNİN İNCELENMESİ

MURAT DİLEK

ÇUKUROVA ÜNİVERSİTESİ
FEN BİLİMLERİ ENSTİTÜSÜ
MAKİNA MÜHENDİSLİĞİ ANABİLİM DALI

Danışman: Doç.Dr. Abdülkadir EKŞİ
Yıl: 2006, Sayfa:74
Juri: Doç.Dr. Abdülkadir EKŞİ
: Prof. Dr. Melih BAYRAMOĞLU
: Doç.Dr. Cengiz D. ATİŞ

Bu çalışmada 5186-H111, 5083-O ve 5083-H111 (Alustar) alüminyum alaşımı levhalar kullanılmıştır. Bağlantıların mekanik ve mikroyapısal özelliklerini incelemek amacıyla alüminyum alaşımı levhalar, birbirlerine aynı ve farklı alaşım çifti olarak Sürtünme karıştırma (FSW) kaynak yöntemiyle, uygun parametreler kullanılarak kaynak edilmişlerdir. Kaynaklı birleştirmelerde metalografik ve mekanik testler yapılarak kaynak ilerleme hızının birleşme bölgesinin metalürjik ve mekanik özelliklerinde meydana getirdiği değişiklikler değerlendirilmiştir. Kaynak edilen levhalardan test edilmek amacıyla numuneler alınarak çekme ve Vickers sertlik ölçümleri yapılmıştır. Kaynak bağlantılarının kaynak bölgesinin mikroyapısal özellikleri Optik Mikroskop (OM) ve Taramalı Elektron Mikroskop (TEM) görüntü analiz sistemi ile detaylı biçimde incelenmiştir.

Anahtar kelimeler: Sürtünme Karıştırma Kaynağı, Al Alaşımlarının Kaynağı,
5186-H111, 5083-O, 5083-H111 (Alustar)

ACKNOWLEDGEMENTS

I am so grateful to my supervisor Assoc. Prof. Dr. Abdülkadir EKŞİ for his guidance, inspiration and encouragement during all my thesis studies.

I also thank my special committee members, my supervisor Assoc. Prof. Dr. Abdülkadir EKŞİ, Prof Dr. Melih BAYRAMOĞLU and Assist. Prof. Dr. Cengiz D. ATİŞ for their enthusiasms and many helpful suggestions.

I would like to thank to all my friends for his endless support: Reaserch Assistant Durmuş Ali BİRCAN and my close friend Mehmet İlteriş SARIGEÇİLİ, Murat BAYSAL, Bilal ÇALIK, Filiz HACIBONCUK, and my brother Süleyman DİLEK.

I would like to thank to Işın Teknik Machine Construction & Textile and Manufacturing Company.

I have to thank to Prof. Dr. Gürel ÇAM in Mustafa Kemal University, Prof. Dr. Adem KURT, Dr. Bülent BOSTAN, Dr. Aydın ŞIK in Gazi University for their special attention during my laboratory works. They have let me use all possibilities of Gazi University Laboratories for microstructure analysis and fatigue test.

Finally, special thanks to my family for their endless supports, and I am so grateful to Reaserch Assistant Durmuş Ali BİRCAN for his endless interest and support during all my thesis studies.

CONTENTS **PAGE**

ABSTRACT I

ÖZ II

ACKNOWLEDGEMENT III

LIST OF TABLES VII

LIST OF FIGURES VIII

NOMENCLATURE XIII

1. INTRODUCTION 1

1.1. Friction Stir Welding Process 1

1.2. Applications of Friction Stir Welding 2

1.2.1. Applications of Friction Stir Welding in Different Geometries 2

1.2.2. Applications of Friction Stir Welding in Aluminum Alloys and Other Materials 3

1.2.3. Applications of Friction Stir Welding in Industry 4

1.3. Advantages of Friction Stir Welding 6

1.4. Limitations of Friction Stir Welding 8

1.5. Microstructural Analysis of Friction Stir Welding 8

1.6. Comparison with Fusion Welding and Friction Stir Welding 10

2. PREVIOUS STUDIES 13

2.1. Friction Stir Welding in a 356 Aluminum Alloy 13

2.2. Friction Stir Welding in 1XXX Series Aluminum Alloys 14

2.3. Friction Stir Welding in 2XXX Series Aluminum Alloys 14

2.4. Friction Stir Welding in 5xxx Series Aluminum Alloys 17

2.5. Friction Stir Welding in 6xxx Series Aluminum Alloys 18
2.6. Friction Stir Welding in 7xxx Series Aluminum Alloys 19
2.7. Friction Stir Welding in Dissimilar Aluminum Alloys 19
2.8. Friction Stir Welding of Aluminum Alloy and Steel 22
2.9. Comparison with Mig, Tig and Friction Stir Welding 23
2.10. Fatigue Properties of Friction Stir Welds in Al Alloys 23
3. MATERIAL AND METHOD 25
3.1. Material 25
3.1.1. Effect of Mg on Strength and Corrosion Resistance 27
3.2. Method 28
3.2.1. Microstructure Analysis 36
3.2.1.1. Optical Microscopy (OM) 36
3.2.1.2. Scanning Electron Microscope (SEM) 37
4. RESULTS AND DISCUSSION 38
4.1. Mechanical Properties 38
4.1.1. Evaluation of Hardness and Tensile Test 38
4.1.2. Evaluation of Fatigue Test 45
4.2. Metallurgical Evaluation 50
4.2.1. Optical Microscope (OM) 50
4.2.2. Scanning Electron Microscope (SEM) 56
5. CONCLUSION AND FUTURE STUDIES 64
5.1. Conclusion 64
5.2. Recommendation of Future Studies 67
REFERENCES 68

CIRRICULUM VITAE..... 74

LIST OF TABLES **PAGE**

Table 3.1. The chemical compositions of each material. 25

Table 3.2. Mechanical properties of each material 27

Table 3.3. Physical properties of AA5083-O and AA5083-H111 Alloys 28

Table 3.4. Combinations of joints. 30

Table 4.1. Ultimate Tensile Stress (UTS) and Yield Stress (YS) diagrams of base, similar joined and dissimilar joined materials. 43

LIST OF FIGURES **PAGE**

Figure 1.1. Schematic illustration of the FSW process 2

Figure 1.2. Schematic illustration of the T-sections..... 3

Figure 1.3. Schematic illustration of welding of
the different aluminum alloys..... 4

Figure 1.4. Friction welded parts including valves and a gearbox fork 5

Figure 1.5. A friction stir welded aluminum wheel..... 5

Figure 1.6. A friction stir welded aluminum connector. 6

Figure 1.7. Schematic illustration of microstructural classification of FSW 9

Figure 2.1. Optical microstructures of the SZ with welding speeds of:
(a) 87 mm min^{-1}, (b) 127 mm min^{-1},
(c) 187 mm min^{-1}, and (d) 267 mm min^{-1} 13

Figure 2.2. Room-temperature (a) and low-temperature
(b) FSW cross sections polished to reveal
the weld zone contrast. Vertical lines denote
weld center line (c)..... 15

Figure 2.3. Hardness variation as a function of lateral distance from
the weld line for each weld at mid-thickness. 18

Figure 2.4. The macro cross-section views of friction stir weld zone.
(a) and (b) are 87 mm/min, (c) and (d) are 187 mm/min,
(e) and (f) are 267 mm/min welding speed, respectively..... 20

Figure 3.1. Reconfigured milling machine used in this study 29

Figure 3.2. Illustration of the tool geometry used in this study..... 29

Figure 3.3. Represented favorable apparatus used in this study..... 30
Figure 3.4. Schematic illustrating the friction stir welding process 31
Figure 3.5. Illustration of distribution planning of the specimens on the sheet material..... 32
Figure 3.6. Dimension of test piece for tensile test used in this study 33
Figure 3.7. Scanning Electron Microscopy (SEM) used in this study. 34
Figure 3.8. High-frequency fatigue test machine used in this study. 35
Figure 3.9. Specimen preparation steps..... 36
Figure 4.1. The variations in Hardness for 5186-H111 / 5186-H111 weld..... 38
Figure 4.2. The variations in Hardness for 5083-O / 5083-O weld..... 39
Figure 4.3. The variations in Hardness for 5083-H111/5083-H111 weld..... 40
Figure 4.4. The variations in Hardness for 5083-O/5186-H111 weld..... 41
Figure 4.5. The variations in Hardness for 5083-O/5083-H111 weld..... 41
Figure 4.6. The variations in Hardness for 5083-H111/5186-H111 weld..... 42
Figure 4.7. Tensile Stress Curves of FS Welded 5186-H111/5186-H111, 5186-H111/5083-O, 5186-H111/5083-H111 Joints..... 43
Figure 4.8. Tensile Stress Curves of FS Welded 5083-O/5083-O, 5083-O/5186-H111, 5083-O/5083-H111 Joints 44
Figure 4.9. Tensile Stress Curves of FS Welded 5083-H111/5083-H111, 5083-H111/5186-H111, 5083-H111/5083-O Joints 44

Figure 4.10. Stress Curves Comparison of FS Welded Joints 45

Figure 4.11. S-N Curve of FS Welded 5186-H111 Base 46

Figure 4.12. S-N Curve of FS Welded 5083-O Base 46

Figure 4.13. S-N Curve of FS Welded 5083-H111 Base 47

Figure 4.14. S-N Curve of FS Welded 5083-O/5083-O Joint 47

Figure 4.15. S-N Curve of FS Welded 5186-H111/5186-H111 Joint 48

Figure 4.16. S-N Curve of FS Welded 5083-H111/5083-H111 Joint 48

Figure 4.17. S-N Curve of FS Welded 5083-O/5186-H111 Joint 49

Figure 4.18. S-N Curve of FS Welded 5083-O/5083-H111 Joint 49

Figure 4.19. S-N Curve of FS Welded 5186-H111/5083-H111 Joint 50

Figure 4.20. Optical Microstructural Analysis of FS Welded 5186-H111 Base (a:10X-b:40X) 51

Figure 4.21. Optical Microstructural Analysis of FS Welded 5083-O Base (a:10X-b:40X) 51

Figure 4.22. Optical Microstructural Analysis of FS Welded 5083-H111 Base (a:10X-b:40X) 52

Figure 4.23. Optical Microstructural Analysis of FS Welded 5083-O/5083-O Joint (a:10X-b:40X) 53

Figure 4.24. Optical Microstructural Analysis of FS Welded 5186-H111/5186-H111 Joint (a:10X-b:40X) 53

Figure 4.25. Optical Microstructural Analysis of FS Welded 5083-H111/5083-H111 Joint (a:10X-b:40X) 54

Figure 4.26. Optical Microstructural Analysis of FS Welded 5083-O/5186-H111 Joint (a:10X-b:40X) 55

Figure 4.27. Optical Microstructural Analysis of FS Welded
5083-O/5083-H111 Joint (a:10X-b:40X)..... 55
Figure 4.28. Optical Microstructural Analysis of FS Welded
5186-H111/5083-H111 Joint (a:10X-b:40X)..... 56
Figure 4.29. SEM Views of Fracture Surfaces of FS Welded
5186-H111 Base (a:40X, 500µm-b:500X, 50µm) 57
Figure 4.30. SEM Views of Fracture Surfaces of FS Welded
5083-O Base (a:40X, 500µm-b:500X, 50µm) 57
Figure 4.31. SEM Views of Fracture Surfaces of FS Welded
5083-H111 Base (a:40X, 500µm-b:500X, 50µm) 58
Figure 4.32. SEM Views of Fracture Surfaces of FS Welded
5083-O/5083-O Joint (a:40X, 500µm-b:500X, 50µm)..... 59
Figure 4.33. SEM Views of Fracture Surfaces of FS Welded
5186-H111/5186-H111 Joint (a:40X, 500µm-b:500X, 50µm)..... 59
Figure 4.34. SEM Views of Fracture Surfaces of FS Welded
5083-H111/5083-H111 Joint (a:40X, 500µm-b:500X, 50µm)..... 60
Figure 4.35. SEM Views of Fracture Surfaces of 5083-O Side of
FS Welded 5083-O/5186-H111 Joint
(a:40X, 500µm-b:500X, 50µm) 60
Figure 4.36. SEM Views of Fracture Surfaces of 5186-H111 Side of
FS Welded 5083-O/5186-H111 Joint
(a:40X, 500µm-b:500X, 50µm) 61

Figure 4.37. SEM Views of Fracture Surfaces of 5083-O Side of FS Welded 5083-O/5083-H111 Joint (a:40X, 500µm-b:500X, 50µm) 61
Figure 4.38. SEM Views of Fracture Surfaces of 5083-H111 Side of FS Welded 5083-O/5083-H111 Joint (a:40X, 500µm-b:500X, 50µm) 62
Figure 4.39. SEM Views of Fracture Surfaces of 5186-H111 Side of FS Welded 5186-H111/5083-H111 Joint (a:40X, 500µm-b:500X, 50µm) 62
Figure 4.40. SEM Views of Fracture Surfaces of 5083-H111 Side of FS Welded 5186-H111/5083-H111 Joint (a:40X, 500µm-b:500X, 50µm) 63

NOMENCLATURE

FSW	Friction Stir Welding
TWI	The Welding Institute
MMC	Metal Matrix Composites
MIG	Metal Inert Gas
SZ	Stir Zone
WN	Weld Nugget
HAZ	Heat and Deformation Affected Zone
TMAZ	Thermo Mechanically Affected Zone
THAZ	True Heat Affected Zone
OM	Optic Microscopy
SEM	Scanning Electron Microscopy
BM	Base Material
HV	Hardness Vickers
X	Distance from Center Line on Retreating Side
X’	Distance from Center Line on Advancing Side
AA	Aluminum Alloy
R	Rotational Speed [mm/min]
WHN	Vickers Hardness Number
EDM	Electro Discharging Machine
R	Retreating Side
A	Advancing Side
TIG	Tungsten Inert Gas

IGC	Inter Granular Corrosion
SCC	Stress Corrosion Cracking
W	Moment of Inertia [mm^3]
σ	Bending Stress [daN/mm^2]
Me	Bending Moment [daN/mm^2]
b	Width [mm]
h	Height [mm]
N_R	Cycles to Rupture
UTS	Ultimate Tensile Strength [MPa]
YS	Yield Strength [MPa]
f	Frequency [s^{-1}]
K_t	Notch Factor
R	Reversing Loading
σ_{min}	Minimum Stress [MPa]
σ_{max}	Maximum Stress [MPa]
σ_{an}	Nominal Stress Amplitude [MPa]

1. INTRODUCTION

1.1. Friction Stir Welding Process

Friction Stir Welding (FSW) is a novel welding technique invented by The Welding Institute (TWI) in 1991 (Cary H.B., 1979). FSW is actually a solid-state joining process that is a combination of extruding and forging and is not a true welding process. FSW is a derivative of conventional friction welding. The FSW process involves the translation of a rotating cylindrical tool along the interface between two plates. The weld is formed by the deformation of the material at temperatures below the melting temperature. FSW does not create a Heat Affected Zone nor does it use welding consumables. Since traditional heating methods are not employed, the properties of the metal in the joined area are higher than those from any other known welding process and distortion is virtually eliminated (Weisheit A. at all, 1998, Juttner S., 1998).

FSW uses a cylindrical, shouldered tool with a profiled pin that is rotated and slowly plunged into the joint line between two pieces of sheet or plate material, which are butted together. The process is solid-state in nature and relies on localized forging of the weld region to produce the joint. The plates comprising the workpiece are held in compression and are rigidly fixtured to the machine bed during welding. Friction stir welding uses a nonconsumable, rotating tool that is cylindrical in shape with a cylindrical pin of smaller diameter extending from the tool shoulder (Thomas, W.M., 1991).

Initially, the rotating tool is plunged into the joint until the shoulder contacts the top surface of the workpiece. Heating is caused by rubbing of the tool faces against the workpiece and by visco-plastic dissipation of mechanical energy at high strain rates developed through interactions with the tool. During welding, the material along the joint is heated to a softened condition, transferred around the periphery of the tool, and subsequently recoalesced along the back surface of the pin to produce the weld.

Schematic illustration of the FSW process is shown in Figure 1.1. Frictional heat is generated between the wear resistant welding tool and the work piece. This heat causes the work piece material to soften without reaching the melting point and allows the tool to traverse the weld line. As it does, the plasticized material is transferred from the leading edge of the tool to the trailing edge of the tool shoulder and pin. It leaves a solid phase bond between the two work pieces.

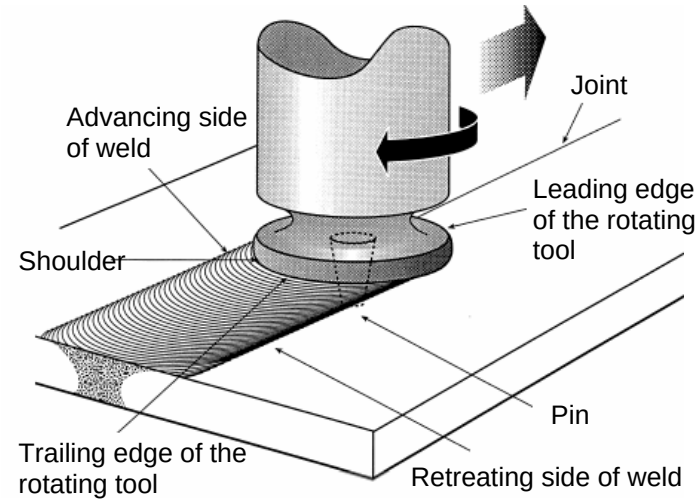


Figure 1.1. Schematic illustration of the FSW process (Thomas W.M., 1991)

1.2. Applications of Friction Stir Welding

1.2.1. Applications of Friction Stir Welding in Different Geometries

The FSW process can also cope with circumferential, annular, non-linear, and three dimensional welds. Since gravity has no influence on the solid-phase welding process, it can be used in all positions:

- Horizontal
- Vertical
- Overhead
- Orbital.

The process has been used for the manufacture of butt welds, overlap welds, T-sections, fillet, and corner welds as shown in Figure 1.2. For each of these joint

geometries specific tool designs are required which are being further developed and optimized (Threadgill P.L., March 1997)

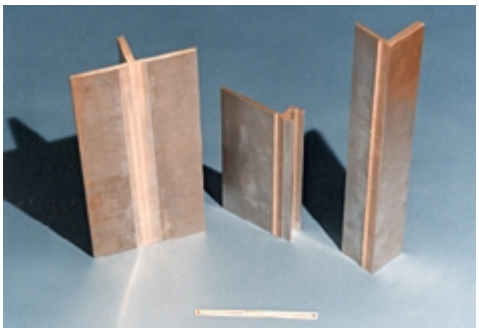


Figure 1.2. Schematic illustration of the T-sections (Cary H.B., 1979).

1.2.2. Applications of Friction Stir Welding in Aluminum Alloys and Other Materials

FSW can be used for joining many types of materials and material combinations. Continuing development of the FSW tool, its design and materials have allowed preliminary welds to be successfully produced in:

- Aluminum alloys 2000 (Al-Cu), 5000 (Al-Mg), 6000 (Al-Mg-Si), 7000 (Al-Zn), 8000 (Al-Li) and other aluminum alloys of the 1000 (commercially pure), 3000 (Al-Mn) and 4000 (Al-Si) series.
- Copper and its alloys
- Lead
- Titanium and its alloys
- Magnesium alloy, magnesium to aluminum
- Zinc
- MMCs based on aluminum (metal matrix composites)
- Plastics
- Mild steel.

FSW has been successfully developed for many non-ferrous alloys, and its feasibility for steels has been demonstrated as shown in Figure 1.3. The process is fully mechanized, needs no traditional welder skills, no consumables, and produces

solid state welds with minimal distortion, and excellent mechanical properties. It is also very useful for joining dissimilar materials.

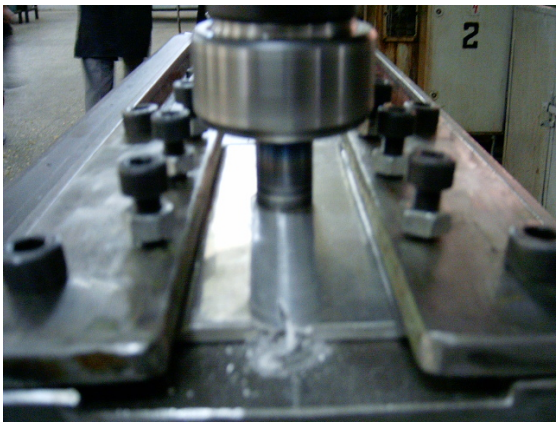


Figure 1.3. Schematic illustration of welding of the different aluminum alloys.

1.2.3. Applications of Friction Stir Welding in Industry

FSW is attractive for the friction heating is generated locally, there is no need the widespread softening of the assembly, the weld is formed across the entire cross-sectional area of the interface in a single shot process, the technique is capable of joining dissimilar materials, the process is completed in a few seconds with very high reproducibility, and suitable for a mass production industry. The process is suitable for the following applications:

Shipbuilding and marine industries include; panels for decks, sides, bulkheads and floors, aluminum extrusions, hulls and superstructures, helicopter landing platforms, offshore accommodation, marine and transport structures, masts and booms, e.g. for sailing boats, refrigeration plant.

Aerospace industry include; wings, fuselages, empennages, cryogenic fuel tanks for space vehicles, aviation fuel tanks, external throw away tanks for military aircraft, military and scientific rockets, repair of faulty MIG welds.

Land transportation include; engine and chassis cradles, wheel rims, attachments to hydroformed tubes, tailored blanks, e.g. welding of different sheet thicknesses, space frames, e.g. welding extruded tubes to cast nodes truck bodies, tail lifts for lorries, mobile cranes, armour plate vehicles, fuel tankers, caravans, buses

and airfield transportation vehicles, motorcycle and bicycle frames, articulated lifts and personnel bridges, skips, repair of aluminum cars, magnesium and magnesium/aluminum joints. The process is also used to fabricate suspension rods, steering columns, gear box forks and drive shafts, as well as engine valves, in which the ability to join dissimilar materials means that the valve stem and head can be made of materials suited to their different duty cycles in service, Figure 1.4. (Jonhson R. at all, 1999).



Figure 1.4. Friction welded parts including valves and a gearbox fork (Jonhson R. et all, 1999)

Wheel assemblies using two aluminum alloys have been made in Figure 1.5., in which the butt or lap welds can be fabricated in wrought and/or cast materials (Jonhson R. et all, 1999).



Figure 1.5. A friction stir welded aluminum wheel. (Jonhson R. et all, 1999)

Construction industry include; aluminum bridges, facade panels made from aluminum, copper or titanium, window frames, aluminum pipelines, aluminum reactors for power plants and the chemical industry, Heat exchangers and air conditioners, pipe fabrication, electrical industry. The Simulform connector has produced for the fabrication of chassis members and space frames, Figure 1.6. FSW has also been used to weld lightweight panels made of plastic foam sandwiched between two sheets of aluminum, for which any fusion welding technique would encounter serious problems because of the much higher temperatures involved. Foamed aluminum itself has been FS welded too. Other current applications under review include the bodies and floors of coaches and buses, military bridge-laying vehicles (and bridges/pontoons), and waste skips (Jonhson R. at all, 1999).

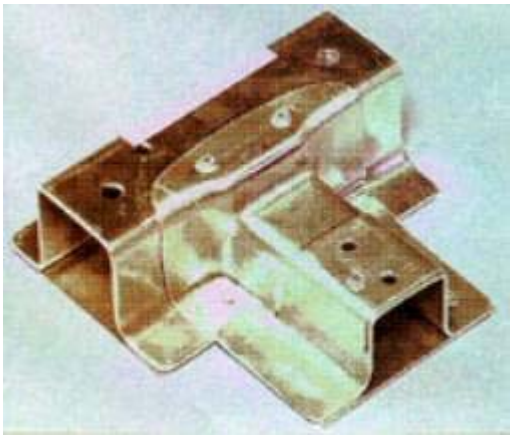


Figure 1.6. A friction stir welded aluminum connector. (Jonhson R. et all, 1999).

Other industry sectors include; refrigeration panels, cooking equipment and kitchens, white goods, gas tanks and gas cylinders, connecting of aluminum or copper coils in rolling mills, furniture.

1.3. Advantages of Friction Stir Welding

The process advantages result from the fact that the FSW process (as all friction welding of metals) takes place in the solid phase below the melting point of

the materials to be joined. The benefits therefore include the ability to join materials which are difficult to fusion weld, for example 2000 and 7000 aluminum alloys.

FSW of dissimilar materials will be required in the near future for advanced automobile and aerospace design. In the present research, we have tried to apply the FSW technique to dissimilar light metals such as 5083 and 5186 aluminum alloys. Then, we have examined the microstructure and the mechanical properties of the welded aluminum alloy joint with various welding speeds.

The process advantages are:

- Low distortion, even in long welds
- Excellent mechanical properties as proven by fatigue, tensile and bend tests
- No fume
- No porosity
- No spatter
- Low shrinkage
- Can operate in all positions
- Energy efficient (Cary H.B., 1979)

FSW can use existing and readily available machine tool technology. The process is also suitable for automation and adaptable for robot use. Its main advantages are:

- Non-consumable tool
- One tool can typically be used for up to 1000m of weld length in 6000 series aluminum alloys
- No filler wire
- No gas shielding for welding aluminum
- No welder certification required
- Some tolerance to imperfect weld preparations - thin oxide layers can be accepted (Cary H.B., 1979)

1.4. Limitations of Friction Stir Welding

The main limitations of the FSW process are:

- Welding speeds are moderately slower than those of some fusion welding processes (up to 750mm/min for welding 5mm thick 6000 series aluminum alloy on commercially available machines)
- Workpieces must be rigidly clamped
- Backing bar required
- Keyhole at the end of each weld (Cary H.B., 1979)

1.5. Microstructural Analysis of Friction Stir Welding

The welds are created by the combined action of frictional heating and mechanical deformation due to a rotating tool. FSW on Al alloys display several microstructurally distinct regions including the Stir Zone (SZ) or Weld Nugget (WN) (along the weld centerline), Heat and Deformation-Affected Zone (HAZ) or Thermo Mechanically Affected Zone (TMAZ) and a True Heat-Affected Zone (THAZ) as shown in Figure 1.7. Microstructural evolution in the different regions of the weld zone is closely linked with the local thermo mechanical cycle experienced during joining.

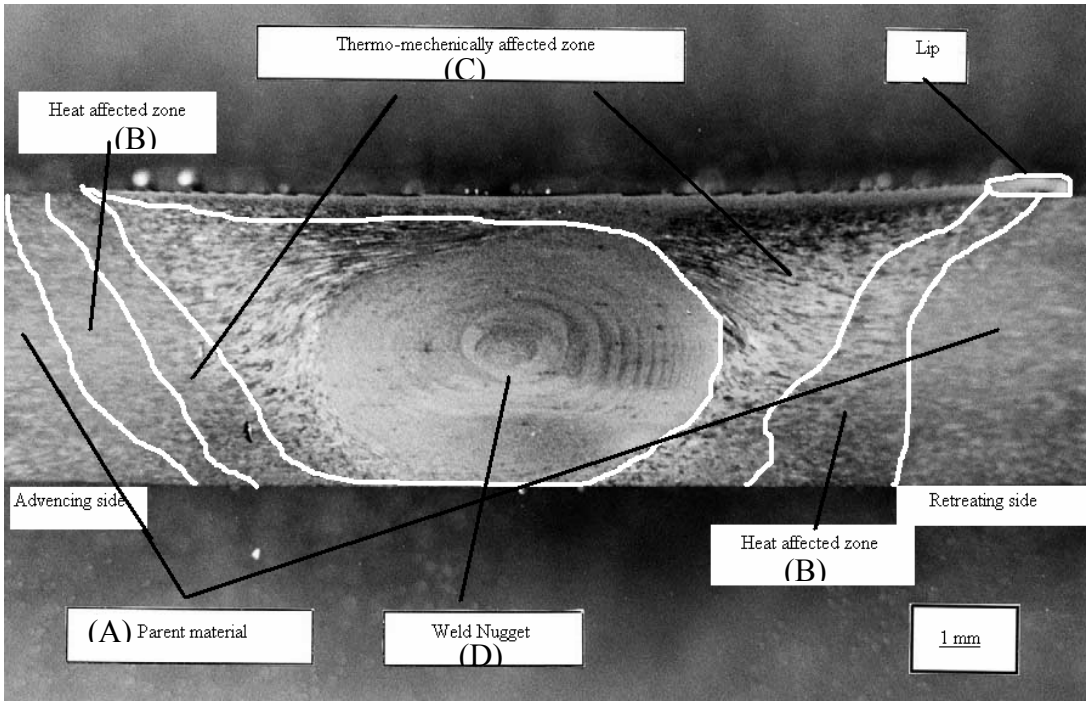


Figure 1.7. Schematic illustration of microstructural classification of FSW

A. Unaffected Material

B. Heat Affected Zone (HAZ)

C. Thermo-Mechanically Affected Zone (TMAZ)

D. Weld Nugget (Part of Thermo-Mechanically Affected Zone)

Unaffected Material or Parent Metal: This is material remote from the weld, which has not been deformed, and which although it may have experienced a thermal cycle from the weld is not affected by the heat in terms of microstructure or mechanical properties.

Heat Affected Zone (HAZ): The material has experienced a thermal cycle which has modified the microstructure and/or the mechanical properties. However, there is no plastic deformation occurring in this area.

Thermo-Mechanically Affected Zone (TMAZ): In this region, the material has been plastically deformed by the FSW tool, and the heat from the process will also have exerted some influence on the material. In the case of aluminum, it is possible to get significant plastic strain without recrystallization in this region, and

there is generally a distinct boundary between the recrystallised zone and the deformed zones of the TMAZ.

Weld Nugget: The recrystallised area in the TMAZ in aluminum alloys has traditionally been called the nugget (Cary H.B., 1979, Threadgill P.L., March 1997)

1.6. Comparison with Fusion Welding and Friction Stir Welding

FSW have been successfully produced on many of the important commercial Al alloys including the 1xxx, 2xxx, 5xxx, 6xxx, and 7xxx. Fusion welds in these alloys can have high defect rates or are too brittle to be useful. Stir welding can be used to join dissimilar aluminum alloys as well. FSW is routinely used to join 2XXX and 7XXX series aluminums. FSW of Al alloys has several advantages over fusion welding processes. FSW offers important advantages over fusion welding, including welding of difficult to weld aluminum alloys (particularly the 7xxx series widely used by aircraft manufacturers), better retention of baseline material properties, fewer welding defects, lower residual stresses, and improved dimensional stability of the welded structure. With FSW, the material being welded doesn't melt or recast. As a result, material transformations that occur during cool down of the weld are in solid state. Another important advantage is FSW joins aluminum alloys fairly rapidly, at about four millimeters per second, with low heat input and without shielding gases and costly filler materials (Air Force Research Laboratory).

FSW does not require consumables in the same sense as fusion welding. The process is autogenous, meaning that filler material is not required. Cover gases are also not required in many cases, although the use of a cover gas has proved beneficial for titanium and steels. Stir welding does not rely on an experienced operator with the right touch, because the process has a near-zero defect rate. Given a well designed and integrated FSW system, the process is extremely robust (Hansen M., 2003).

First, problems with solidification cracking, liquation cracking, and porosity are eliminated due to the solid state nature of the process. Consequently, FSW permits joining of most of the Al alloys, including those considered unweldable with

fusion welding processes. Moreover, FSW often exhibit improved mechanical properties relative to those of fusion welds on the same material. Finally, residual stresses and distortion in FSW are typically lower than those of fusion welds. The improvements in mechanical properties, residual stresses, and distortion relative to fusion welding are thought to stem from the lower heat input inherent with FSW. The joints also have much higher elongation than fusion welding, as much as two or three times more, depending on the alloy and heat treatment. This higher elongation increases the energy absorption in the weld prior to failure, which is beneficial for high shock applications (Hansen M., 2003).

A number of potential advantages of FSW over conventional fusion welding processes have been identified;

- Improved safety due to the absence of toxic fumes or the spatter of molten material.
- Good mechanical properties in the as welded condition.
- Unlike fusion welding, stir welding does not emit radiation, so welding curtains and face shields are not required.
- No consumables, conventional steel tools can weld over 1000m of aluminum and no filler or gas shield is required for aluminum.
- Easily automated on simple milling machines lower set up costs and less training.
- Can operate in all positions (horizontal, vertical, etc), as there is no weld pool.
- Generally good weld appearance and minimal thickness under/over matching, thus reducing the need for expensive machining after welding.
- Low environmental impact.
- Since the process is solid state, the joint is not subject to any shrinkage as a result of phase changes. The process also introduces minimal heat into the weld, so the heat affected zone is relatively small in comparison to arc welding (Nicholas E.D., 1998).

However, some disadvantages of the process have been identified:

- Exit hole left when tool is withdrawn.

- Large down forces required with heavy duty clamping necessary to hold the plates together.
- Less flexible than manual and arc processes (difficulties with thickness variations and non-linear welds).
- Often slower traverse rate than some fusion welding techniques although this may be offset if fewer welding passes are required (Nicholas E.D., 1998).

In this study, 5186-H111, 5083-O and 5083-H111 aluminum alloy plates were welded as similar and dissimilar alloy joints using Friction Stir Welding (FSW) process in order to investigate mechanical and microstructural properties. In order to investigate the effect of welding speeds on mechanical properties, metallographic and mechanical tests were carried out on the welded areas of the parts. Vickers hardness profile, tensile tests and fatigue tests of the joints experimentally assessed. As a metallurgical investigation, Optic Microscopy (OM) and Scanning Electron Microscopy (SEM) were used for base and weld zones.

2. PREVIOUS STUDIES

2.1. Friction Stir Welding in a 356 Aluminum Alloy

Lee W.B. et all (2003) studied the improvement of mechanical properties of Friction Stir welded A356 Al alloy with 87 mm min^{-1}, 127 mm min^{-1}, 187 mm min^{-1}, and 267 mm min^{-1} FSW speeds. Figure 2.1 shows the optical microstructural changes of the SZ with welding speeds. The Si particles have been homogeneously distributed in the whole SZ regardless of the welding speeds, but the portion of the Si particles in the SZ decreases as welding speed increases.

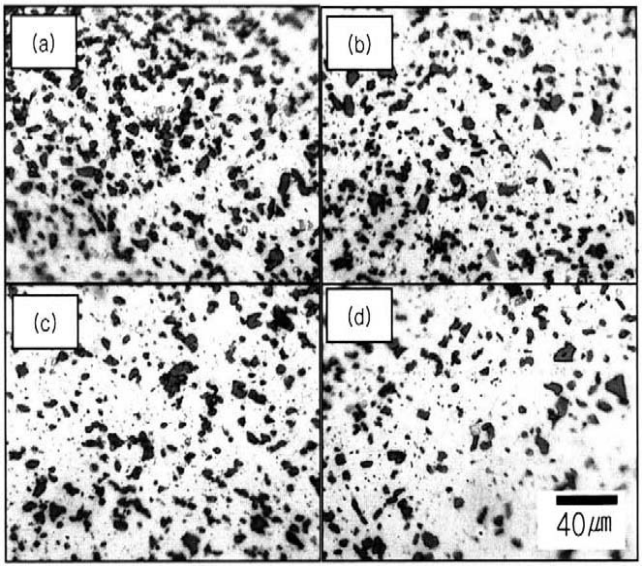


Figure 2.1. Optical microstructures of the SZ with welding speeds of: (a) 87 mm min^{-1}, (b) 127 mm min^{-1}, (c) 187 mm min^{-1}, and (d) 267 mm min^{-1} (Lee, 2003).

The variation of hardness profiles along the centerline of the cross section of the welds with various welding speeds have been researched. The BM has a range of hardness, approximately from 50 to 64 HV. The BM had a hypoeutectic Al-Si microstructure. The Al solid solution, which is softer than the Si solid solution, has a large volume fraction. If the measured hardness indenter has been located more near a primary phase than near eutectic Al-Si, the hardness is about 50 HV, but in the opposite case, the hardness of the BM shows over 60 HV. The hardness of BM depends on the measured point of the hardness indenter. However, the hardness of

the SZ shows more uniform values than that of the BM due to finer and uniformly dispersed Si particles. The transverse ultimate and yield strength had similar values with the BM. All the specimens have been fractured at the unaffected BM. The longitudinal ultimate tensile strength has over 178 MPa, which is 20% improvement of that of the BM, and the yield strength also shows higher value. The mechanical properties of the SZ have been improved by the dispersed Si particles and the homogeneous microstructure compared with that of BM.

2.2. Friction Stir Welding in 1XXX Series Aluminum Alloys

Sato Y.S. et all (2003) studied a friction stir welding of ultrafine grained Al alloy 1100 produced by accumulative roll bonding. FSW resulted in reproduction of fine grains in the stir zone and small growth of the ultrafine grains of the ARBed material just outside the stir zone. FSW suppressed large reductions of hardness in the ARBed material, although the stir zone and the TMAZ experienced small reductions of hardness due to dynamic recrystallization and recovery. Consequently, FSW effectively prevented the softening in the ARBed alloy.

2.3. Friction Stir Welding in 2XXX Series Aluminum Alloys

Benavides S. et all (1999) studied a low temperature FSW of 2024 aluminum. They have been demonstrated to involve dynamic recrystallisation producing ultra-fine, equiaxed grain structures to facilitate superplastic deformation as the welding or joining mechanism. Author obtained that 2024 Al alloy has been FS welded at a starting temperature of 230°C, and maximum weld zone temperatures did not exceed about 140°C. The residual FSW zone grain structure consisted of equiaxed, fine grains having a uniform size of about 0.8 mm throughout. This compares with a central weld zone grain size of about 10 mm in 2024 Al FSW at a starting temperature of 30°C, where the maximum weld zone temperature was measured to be 330°C.

Figure 2.2.a and b show for comparison polished and etched FSW cross sections of 2024 aluminum from room temperature (Figure 2.2.a) and low temperature (Figure 2.2.b) welds. Figure 2.2.c shows corresponding microhardness traverses along the reference lines indicated by the arrows in Figure 2.2.a and b. It is apparent on comparing Figure 2.2.a and b that the weld efficiency, as represented by the tunnel defect shown (arrow), declines appreciably at low temperature. Correspondingly, the microhardness profiles shown in Figure 2.2.c reflect the narrowing of the weld zone at low temperature, and especially a reduction of the HAZ or stir affected zones. There is a noticeable reduction in the softening near the weld zone boundary on either side of the weld HAZ at low temperature, even though there is no corresponding softening in the weld zone itself in contrast to the room temperature weld zone. This effect tends to create an apparent hardness inversion in the corresponding weld zones in Figure 2.2.c.

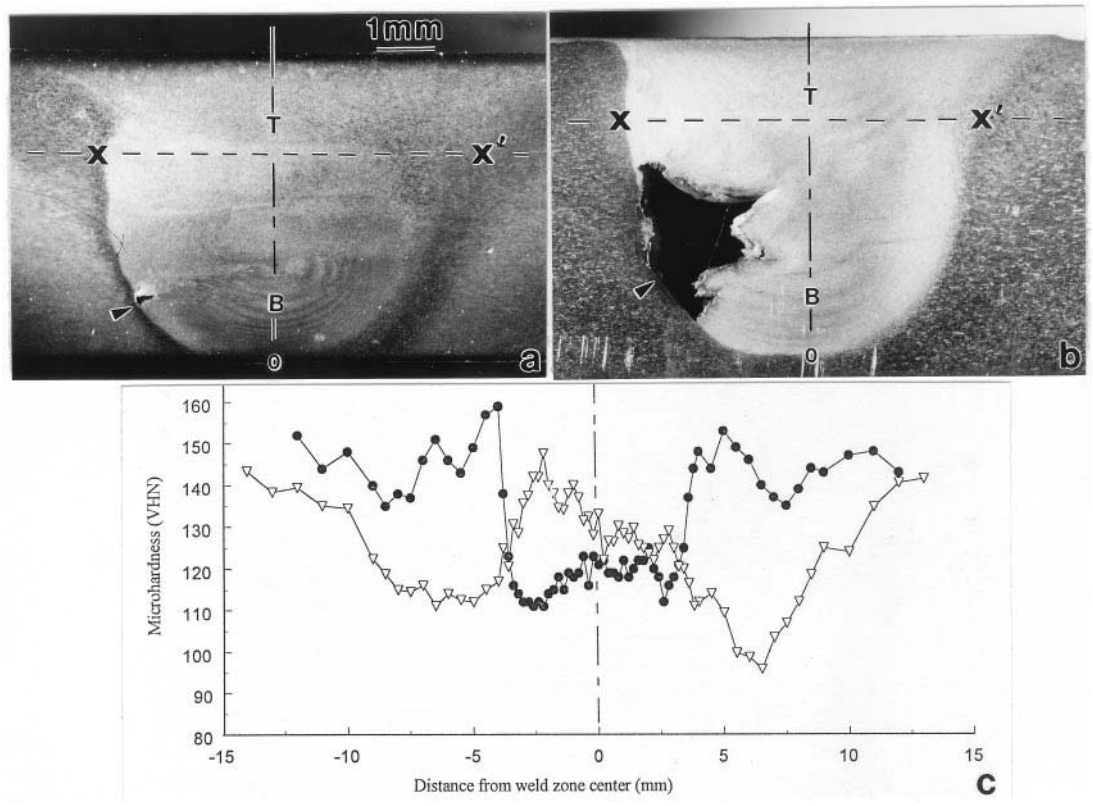


Figure 2.2. Room temperature (a) and low-temperature (b) FSW cross sections polished to reveal the weld zone contrast. Vertical lines denote weld center line. (c) Corresponding and comparative microhardness scans across the cross sections as noted by the arrows (marked X and X') and dotted paths shown in (a) and (b). Open

triangles are room-temperature data; solid circles are low-temperature data (Benavides, 1999)

Salem H.G. (2003) used friction stirring technology to join dynamically recrystallized Al base thin sheets for structural parts brought about the need for the macro and microstructural evolution and hardness characterization. FSW at 1000 rpm rotational speeds and 4.2 mm/s feeding rate have been successfully performed with almost no grain growth for the welds. FSW augmented the formation of fine equiaxed structure with high grain boundary misorientation angles. The thermal and mechanical effect associated with FSW controlled the particle size and distribution within the weld nugget and hence the hardness profile. FSW has proven its capability of creating very fine grain structures in the stirred region. This result from the intense plastic straining associated with the movement of material from the front to the back of the rotating pin. Because of the frictional effect as well as shear deformation, the material undergoes localized heating and hence relative softening, which facilitates plastic deformation.

Fonda R.W. et all (2004) studied a development of grain structure during friction stir welding. They stated that a stop action friction stir weld has been prepared in Al–Li 2195 to ‘‘freeze in’’ the dynamic deformation field surrounding the FSW tool. Analysis of a plan view section of this weld reveals important new details of the grain structure evolution and texture development occurring around the FSW tool. Bands of refined grains develop ahead of the fully refined region, likely reflecting different relative stabilities of the original grain orientations to the applied deformation. Fine subgrains form in response to the predominantly simple shear deformation field and gradually develop greater misorientations to produce the refined grains observed adjacent to the tool. This region displays a typical fcc shear texture after suitable rotations are applied. The primary mechanism of grain refinement in this weld, therefore, appears to be subdivision induced by deformation and dynamic recovery processes, without the need to invoke a dynamic recrystallization mechanism.

Dickerson T. et all (2003) studied a weld marker technique for flow visualization in friction stir welding. They stated that the techniques are based on the

use of a marker material that has been redistributed during welding. Copper strips (0.1mm thick) have been used as markers. After welding various methods have been used to investigate the marker movement including; radiography, tomography and metallurgical sectioning.

Sutton M.A. et all (2004) studied a banded microstructure in 2024-T351 and 2524-T351 aluminum friction stir welds for mechanical characterization. They stated that a series of micro mechanical experiments have been performed to quantify how the FSW process affects the material response within the periodic bands. Micro mechanical studies employed sectioning of small samples and micro tensile testing using digital image correlation to quantify the local stress–strain variations in the banded region. Results indicate that the two types of bands in 2024-T351 and 2524-T351 aluminum FSW joints have different hardening rates with the particle-rich bands having the higher strain hardening exponent, exhibit a periodic variation in micro hardness across the bands and the individual bands in each material have the same initial yield stress. They heve been obtained that periodic characteristics in the banded microstructure seem to be inherent in the FSW process, with a direct and consistent relationship observed between periodicity in the metallurgical and mechanical behavior (e.g. grain size, particle distribution, band width, micro hardness, strain) and the tool advance per revolution during the welding process.

2.4. Friction Stir Welding in 5xxx Series Aluminum Alloys

Peel M. (2003) studied a microstructure, mechanical properties and residual stresses as a function of welding speed in aluminium AA5083 friction stir welds. It has been found that the weld properties have been dominated by the thermal input rather than the mechanical deformation by the tool.The main results have been obtained that the recrystallisation results in the weld zone having considerably lower hardness and yield stress than the parent AA5083. During tensile testing, almost all the plastic flow occurs within the recrystallised weld zone. The peak longitudinal stresses increase as the traverse speed increases. This increase is probably due to steeper thermal gradients during welding and the reduced time for stress relaxation to

occur. The base material is in an extremely work hardened state and this is reflected in the hardness profiles shown in Figure 2.3.

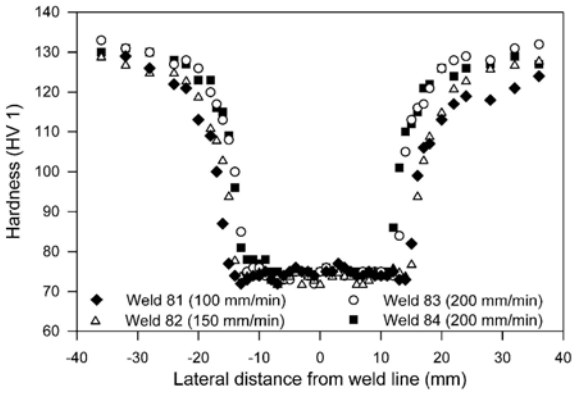


Figure 2.3. Hardness variation as a function of lateral distance from the weld line for each weld at mid-thickness (Peel M., 2003).

2.5. Friction Stir Welding in 6xxx Series Aluminum Alloys

Liu G. et all (1997) studied microstructural aspects of the friction stir welding of 6061-T6 aluminum. They stated that LM and TEM have been used to characterize the microstructures in the FS weld zone and calmpare them with the original 6061-T6 60 aluminum alloy plate (nominally 0.63 cm thick) have been used. They have also measured the associated microhardness profile extending from the workpiece and through the weld zone.A series of butt welds and simulated welds in solid plate sections have been conducted, at rotational speeds (R) ranging from 300 to 1000 rpm, and translational (traverse) velocities of 0.15 to 0.25 cm/s. The hardened carbon steel welding head pin was 0.63 cm in diameter and its length was 58 cm. The main results have been obtained that the FS weld zone in 6061-T6 aluminum is characterized by what appears to be a dynamic continuous recrystallization microstructure. Second phase particles in the workpiece are essentially “stirred” into the weld zone where the residual hardness varies from 55 WHN near the top of the weld to 65 WHN near the bottom; in contrast to a workpiece hardness which varies

between about 85 and 100 WHN. The weld zone grain size averaged 10 μm in contrast to 100 μm for the workpiece.

2.6. Friction Stir Welding in 7xxx Series Aluminum Alloys

Rhodes C.G. et all (1996) studied effects of FSW on microstructure of 7075 aluminum. They stated that the technique, based on friction heating at the faying surfaces of two pieces to be joined, results in a joint created by interface deformation, heat, and solid-state diffusion. The weld is characterized by a recrystallized nugget having a 2-4 μm grain size. The dislocation density in the nugget is lowered from that in the parent metal; strengthening precipitates appear to have been solutionized during the welding process, with the larger ones re-precipitating on cooling. The process, thus, provides a method for joining an unweldable aluminum alloy without introducing a cast microstructure.

2.7. Friction Stir Welding in Dissimilar Aluminum Alloys

Lee W.B. et all (2003) studied joint properties of dissimilar formed Al alloys by FSW according to the fixed location of materials. They stated that the mechanical properties of the weld mainly depended on the materials fixed at the retreating side because the microstructure of the stir zone was mainly composed of the materials fixed at the retreating side. A356 Al alloy have been used and wrought 6061 Al alloy which size is 140 mm in length, 70 mm in width and 4 mm in thickness. To determine the tensile strength of the stir zone, tensile test specimens have been sectioned in the longitudinal direction to the weld line with an EDM. Microstructural changes from the weld zone to the unaffected base metal have been examined with OM and SEM.

Figure 2.4. illustrates the macro images of the weld zone with 87 mm/min, 187 mm/min and 267 mm/min welding speeds. From the different etching response of each material, 6061 Al alloys appeared darker colored than A356 Al alloys in the stir zone. In case A356 Al alloys were fixed at the retreating side, more light colored

regions that have been estimated as that of A356 Al alloys occupied the large fraction in the stir zone. However, when 6061 Al alloys have been fixed at the retreating side, the microstructure of the stir zone have been mainly composed of that of 6061 Al alloys. Therefore, the macrostructure of the stir zone mainly depended on the materials fixed at the re-treating side and some of the advancing sided material.

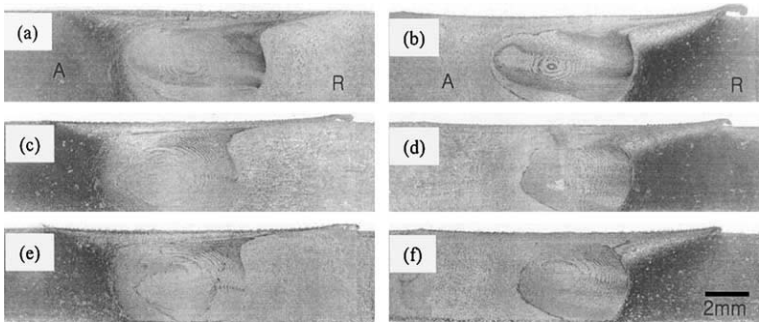


Figure 2.4. The macro cross section views of friction stir weld zone. (a) and (b) are 87 mm/min, (c) and (d) are 187 mm/min, (e) and (f) are 267 mm/min welding speed, respectively. Left figures are A356 fixed at the retreating side and right figures are 6061 fixed at the retreating side. (*R*) represents retreating side and (*A*) represents advancing side. (Lee, 2003)

The main results have been obtained that the microstructures of dissimilar formed A356/ 6061Al joint showed the mixed structures of two materials. The onion ring pattern, which appeared like lamellar structure, has been observed in the stir zone. The microstructure of the stir zone has been mainly composed of the material fixed at the retreating side. The mechanical properties of the stir zone showed higher value when 6061 Al alloys has been fixed at the retreating side.

Wert J.A. studied microstructures of FSW joints between an aluminium-base metal matrix composite and a monolithic aluminium alloy. They stated that microstructures in FS welds between monolithic AA2024 and AA2014 reinforced with 20 vol % particulate Al_2O_3 reveal that the narrowest layers of each material are about 0.1 mm thick. Thus, each material retains its identity in the weld zone and convoluted macrointerfaces can be identified between material domains. When the harder material is on the advancing side of the tool the macrointerface span is larger; this can be understood qualitatively by considering how the relative hardness affects material transport. The welds also exhibit eutectic melting. The liquid phase has the

traditional form of grain boundary films in the thermomechanical process zone. Particle strings and fragmentation fracture zones have been observed; these may also result from eutectic melting.

Cavaliere P. et all (2006) studied a mechanical and microstructural behaviour of 2024–7075 aluminium alloy sheets joined by friction stir welding. The resulted microstructure due to the FSW process has been studied by employing OM and SEM either on 'as welded' specimens and on tested specimen after rupture occurred. The main results have been obtained that the dissimilar 2024 and 7075 aluminium alloys in the form of 2.5 mm thick sheets have been successfully joined by friction stir welding.. The specimens fracture surfaces after testing have been deeply analysed by using a FEGSEM microscope, revealing the defects typology and location after the friction stirring process and the microscopic mechanisms occurred during high stress deformations and final failure.

Jata K.V. et all (2006) studied a continuous dynamic recrystallization during FSW of high strength aluminum alloys. They stated that the stir welded plates of an Al-Li-Cu alloy (Al-1.8 Li-2.7Cu-0.33Mg-0.33Mn-0.04 Zr-0.7Zn) have been used which had been hot rolled, homogenized, solution heat treated, water quenched, and naturally aged prior to joining. OM has beeen performed to reveal the general microstructure of the weld and the base metal.

Li Y. et all (1999) studied a flow visualization and residual microstructures associated with the friction stir welding of 2024 aluminum to 6061 aluminum. They stated that the FSW of 0.6 cm plates of 2024 Al (140 HV) to 6061 Al (100 HV) is characterized by residual, equiaxed grains within the weld zone having average sizes ranging from 1 to 15 mm, exhibiting grain growth from dynamically recrystallized grains which provide a mechanism for superplastic flow; producing intercalated, lamellar like flow patterns. These flow patterns are visualized by differential etching of the 2024 Al producing contrast relative to 6061 Al. The equiaxed grain and sub-grain microstructures have been observed to vary according to estimated temperature profiles referenced to the rotating tool axis. Dislocation spirals and loops have been also observed in the 2024 Al intercalation regions within the weld zones at higher speeds (> 800 rpm) corresponding to slightly elevated temperatures introducing

dislocation climb, and residual microhardness profiles follow microstructural variations which result in a 40% reduction in the 6061 Al workpiece microhardness and a 50% reduction in the 2024 Al workpiece microhardness just outside the FSW zone.

Chao J. et all (2001) studied the effect of FSW on dynamic properties of AA2024-T3 and AA7075-T7351. Dynamic, compressive stress-strain curves have been obtained of AA2024-T3 and AA7075- T7351 aluminum alloys and their welds as produced by the FSW process. The experimental results have been obtained that the FSW reduces the yield stress of the weld metal to below that of the base metal, both materials exhibit the strain rate effect. Yield stresses of both base and FS welded material of AA2024-T3 exhibited rate sensitivity. In addition, AA7075-T7351 base metal had some rate dependence. However, no rate effect have been found for AA7075-T7351 FS welded material up to the strain rate of 500/s. FSW reduced the yield stress of both AA2024-T3 and AA7075-T7351 under both high strain rate and quasistatic loading conditions.

2.8. Friction Stir Welding of Aluminum Alloy and Steel

Chen C.M. et all (2004) studied a joining of Al 6061 alloy to AISI 1018 steel by combined effects of fusion and solid state welding. The process has been derived from FSW but with an adjustable offset of the probe location with respect to the butt line. Metallographic studies by OM, EDM, and the utilization of the X-ray diffraction technique have been conducted. It has been found that the intermetallic phases $Al_{13}Fe_4$ and Al_5Fe_2 exist in the weld zone.

2.9. Comparison with MIG, TIG and Friction Stir Welding

Ericsson M. et all (2003) studied influence of welding speed on the fatigue of friction stir welds, and comparison with MIG and TIG. They also have been investigated to determine whether the fatigue strength of FS welds is influenced by the welding speed, and also to compare the fatigue results with results for conventional arc welding methods: MIG pulse and TIG. The Al–Mg–Si alloy 6082 was FS welded in the T6 and T4 temper conditions, and MIG-pulse and TIG welded in T6. The T4-welded material has been subjected to a post weld ageing treatment. They have been concluded that at a significantly lower welding speed, the fatigue performance has been improved possibly due to the increased amount of heat supplied to the weld per unit length. The MIG pulse and TIG welds showed lower static and dynamic strength than the FSW. The TIG welds had better fatigue performance than the MIG pulse welds. The experimental results have been obtained that the fatigue strength of FS welded Al–Mg–Si alloy 6082 is higher than that of MIG pulse and TIG welds of the same material. The TIG welds show better fatigue performance than MIG.

2.10. Fatigue Properties of Friction Stir Welds in Al Alloys

Zhou C. et all (2005) studied the fatigue properties of friction stir welds in Al 5083 alloy and inert gas metal arc welding (MIG pulse). The fatigue life of friction stir welds is 9–12 times longer than that of MIG pulse welds under R = 0.1 and the fatigue characteristic values of each welds have been increased from 39.8 MPa for MIG to 67.3 MPa for FSW. The experimental results have been obtained that for all the fractured specimens, cracks initiated from the root part of the FSW, and may have been caused by imperfection in the root of weld. The relative difficulty of detecting defects in FSW makes it necessary to fully understand the influence of any defects on the fatigue property of FSW in the future.

Dickerson T.L. et all (2003) studied the fatigue of friction stir welds in aluminium alloys that contain root flaws. The monotonic strength and fatigue

behaviour of single-sided butt welds in 6–7 mm thick AA5083-O, AA5083-H321 and AA6082-T6, both without and with root flaws, have been investigated. Welding has been carried out to deliberately produce joints both without (flaw-free) and with (flawed) root flaws. Three parent materials have been welded to themselves: AA5083-O, AA5083-H321 and AA6082-T6.

They have reported that the root flaws in the 5083-O and the 6082-T6 welds did not induce a significant loss in static or fatigue strength compared to similar welds without root flaws. The larger root flaws in the 5083-H321 welds caused a reduction in the ultimate tensile strength and ductility when compared to welds without flaws. SEM analyses of exposed root flaw surfaces revealed partial bonding. The bonding increased with increasing distance from the weld root. There has been limited evidence that the partial bonding at the root flaw interface can delay fatigue cracking, however, there are insufficient data to make a definitive statement. Therefore, any root flaw that affects tensile properties or is deeper than 0.35 mm should be assumed unbonded from the outset of any loading.

3. MATERIAL AND METHOD

3.1. Material

Aluminum alloys are preferred to be used in automotive, machine and train body structure due to their lightweight properties plus suitability of their mechanical properties required by the related industries. Main problem to be tackled in using these alloys is the difficulties encountered during welding process. It is very difficult to join these alloys by conventional welding techniques. Additionally mechanical properties of welded alloy obtained in conventional welding process are far from the required values.

The materials used in this study were 5083-O, 5186-H111 and 5083-H111 (Alustar) Aluminum alloys which size is 5 mm in thickness 190 mm in length and 90 mm in width. The chemical compositions are listed in Table 3.1.

Table 3.1. The chemical compositions of each material

	Si	Fe	Cu	Mn	Mg	Cr	Zn
5186-H111	0,190	0,360	0,100	0,320	4,670	-	-
5083-O	0,400	0,262	0,027	0,035	4,759	0,094	0,004
5083-H111 (Alustar)	0,580	0,107	0,021	0,748	5,407	0,008	0,596

The major alloying element of 5000 series is Magnesium. Magnesium is one of the most effective and widely used alloying elements for aluminum. When it is used as the major element, the result is a moderate to high strength non-heat treatable alloy. Alloy in this series possess good welding characteristics and good resistance to corrosion in marine atmosphere. Since 5000 series alloys are designed as non-heat treatable alloys further strength can be obtained by temper treatment. As one of the higher Magnesium content (Al-4.5 Mg) alloy in 5000 series 5083-H111 aluminum alloy is designed as a moderate strength non-heat treated Al-Mg alloy. H111 temper designation indicates strain hardened and then stabilized by tempering at a low

temperature to increase ductility at the cost of a small reduction in strength. 5083-H111 is a Magnesium based aluminum alloy, with additional alloying elements Mn, Cr and Si. It has been indicated that Cr and Mn or combination of these two elements are added to aluminum alloys as stress corrosion control elements, both elements being effective in reducing grain boundary β-phase precipitation and increasing recrystallization temperature. They also increase strength at the expense of a certain amount of ductility and form ability. The presence of Si helps to increase fluidity, which is important in welding and reduces solidification and hot-cracking tendencies.

The base material was a AA5083-O sheet of 5 mm thickness having the nominal composition (weight %) 4–4.9% Mg, 0.4–1% Mn, 0.05–0.25% Cr, balance Al. This alloy has a relatively large Mg content to promote solid solution strengthening and to increase the rate of work hardening, the most important strengthening mechanisms in this alloy (Polmear I.J., 1995). Manganese is present to increase the recrystallization temperature and to improve the strengthening effect of the magnesium. This alloy designation was originally intended for super plastic forming and had been very heavily deformed in order to produce a fine recrystallised grain size upon annealing.

AA5083-H111 is the most heavily consumed non-ferrous metal in the world. Its unique properties such as light weight, high strength and resistance to corrosion make it an ideal material for use in conventional and novel applications. AA5083-H111 has already become important in the production of automobiles, aerospace parts and the manufacture of machinery. AA5083-H111 users have to explore new process technologies in order to reduce production costs and make AA5083-H111 even more competitive (Totton G.E. at all, 2003). Mechanical properties of each material are shown in Table 3.2.

The base material was a AA5186-H111 sheet of 5 mm thickness having the nominal composition (weight %) 3.8–4.8% Mg, 0.2–0.5% Mn, 0.05–0.15% Cr, balance Al.

Table 3.2. Mechanical properties of each material

Material	Tensile Strength (MPa)		Proof Strength (MPa)	Elongation (%)
	Min	Max	Min	
5186-H111	220	280	145	30
5083-O	275	350	125	17
5083-H111	260	330	160	24

3.1.1. Effect of Mg on Strength and Corrosion Resistance

Among all aluminum alloys, the non-heat treatable Al-Mg alloys (5xxx series) are the most suitable material for marine applications. Magnesium, as the main alloying constituent, lends itself to reasonable strength for marine applications. More important, however, is the corrosion resistance of Al-Mg alloys which makes them the most suitable material for shipbuilding.

The relationship between Magnesium content of 5xxx alloys and its mechanical properties, i.e. yield strength, tensile strength, and elongation. The main reason for increasing strength is the formation of Al-Mg intermetallic particles which reinforce the alloy.

Theoretically, increasing the Mg content will add to strength. However, when Mg% is raised above approximately 4%, the corrosion resistance of the alloy will gradually decrease. The reason for this phenomenon is that at higher Mg%, the Al-Mg intermetallic particles will start precipitating at the grain boundaries. These particles are anodic relative to Aluminum and thus they cause electrochemical imbalance in the grains which leads to “Inter Granular Corrosion, (IGC)”. This causes pitting and weight loss. Furthermore, IGC may lead to “Stress Corrosion Cracking, (SCC)”. Physical properties of AA5083-O and AA5083-H111 alloys shown in Table 3.3.

Table 3.3. Physical properties of AA5083-O and AA5083-H111 Alloys

Properties	AA5083-O	AA5083-H111
Density at 20°C [g/cm³]	2.66	2.64
Approximate Melting Range [°C]	574-638	568-636
Coefficient of Linear thermal Expansion [µm/m.K] (20-200°C)	25.0	24.5
Specific heat at 20°C [J/kg.K]	900	890
Electrical conductivity at 20°C [%IACS]	29	27.1
Electrical resistivity at 20°C [µWcm]	5.95	6.3

3.2. Method

FSW has many welding parameters, such as tool (shoulder and screw like probe) materials, tool rotation speed, welding speed and the angle of the tool. In this study, in the first step, aluminum sheet materials 5186-H111, 5083-O, 5083-H111 (Alustar) and the combinations, 5083-O/5083-O, 5186-H111/5186-H111, 5083-H111/5083-H111 and 5083-O/5186-H111, 5083-O/5083-H111, 5186-H111/5083-H111 had dimensioned in 90mm×190mm×5mm, were joined in 20, 50, 80 mm/min welding speed by reconfigured milling machine in Figure 3.1.

In all cases, other parameters were fixed at 1400 rpm of the tool rotation speed and the tool was tilted at 3° from the plate normal, such that the rear of the tool was lower than the front and had a shoulder plunge depth of 0.55 mm below the plate surface. The welding tool was rotated in the clockwise direction and specimens, which were tightly fixed at the backing plate, were travelled. The test piece was fixed onto a steel plate horizontally. Welding direction was perpendicular to the rolled direction of the aluminum plates.



Figure 3.1. Reconfigured milling machine used in this study

The tool had an 18 mm diameter shoulder and a standard metric M5 threaded pin (5 mm wide and 0.8 mm pitch) as shown in Figure 3.2.



Figure 3.2. Illustration of the tool geometry used in this study.

A favorable apparatus was designed for fix the sheet material to reconfigured milling machine as shown in Figure 3.3.

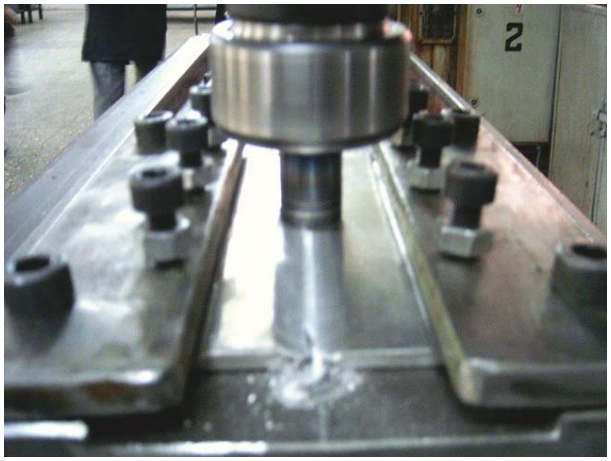


Figure 3.3. Represented favorable apparatus used in this study.

Table 3.4. shows combinations of test pieces. Following FSW, microstructures of the samples were observed by optical microscopy.

Table 3.4. Combinations of joints.

No	Plate 1	Plate 2
No.1	5186-H111	5186-H111
No.2	5083-O	5083-O
No.3	5083-H111	5083-H111
No.4	5083-O	5186-H111
No.5	5083-O	5083-H111
No.6	5186-H111	5083-H111

The both side of the weld zone divided into the retreating side and the advancing side from the relation between the tool rotation direction and plate travel direction. Two kinds of tensile test specimens were sectioned from the welded specimens. One is transverse (A) to the weld zone and the other is longitudinal (B) to the weld zone as shown in Figure 3.4. Distribution planning of the specimens on the

sheet material is shown in Figure 3.5. Microstructural changes from the weld zone to the unaffected BM were examined with OM and SEM.

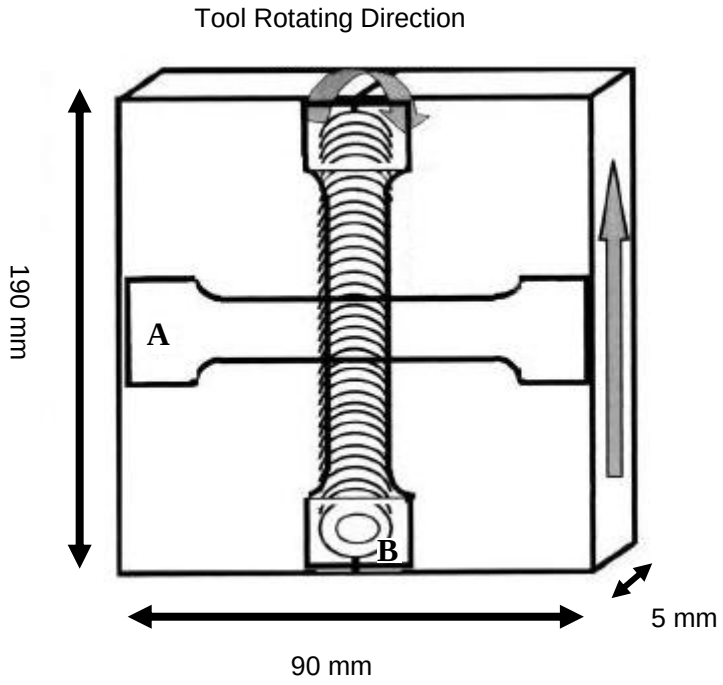


Figure 3.4. Schematic illustration of friction stir welding process. Retreating side is anti-parallel relation between tool rotation direction and plate travel direction.

Macro views of tensile test samples were obtained with the OM. Values of yield strength and ultimate tensile strength of each material were obtained with their graphics in Adana KOSGEB.

The Vickers hardness profile of the weld zone (HV or VHN) was measured on a cross-section and perpendicular to the welding direction using a Vickers indenter with a 100 gf load for 10 s. The hardness profile values of tensile test samples for each main material were obtained with OM and changes over the hardness profile values were plotted in laboratory of mechanical engineering department. These measurements were made above the mid-section and extended from the base metal, through the FSW zone, and into the base metal on the opposite side of the weld zone.

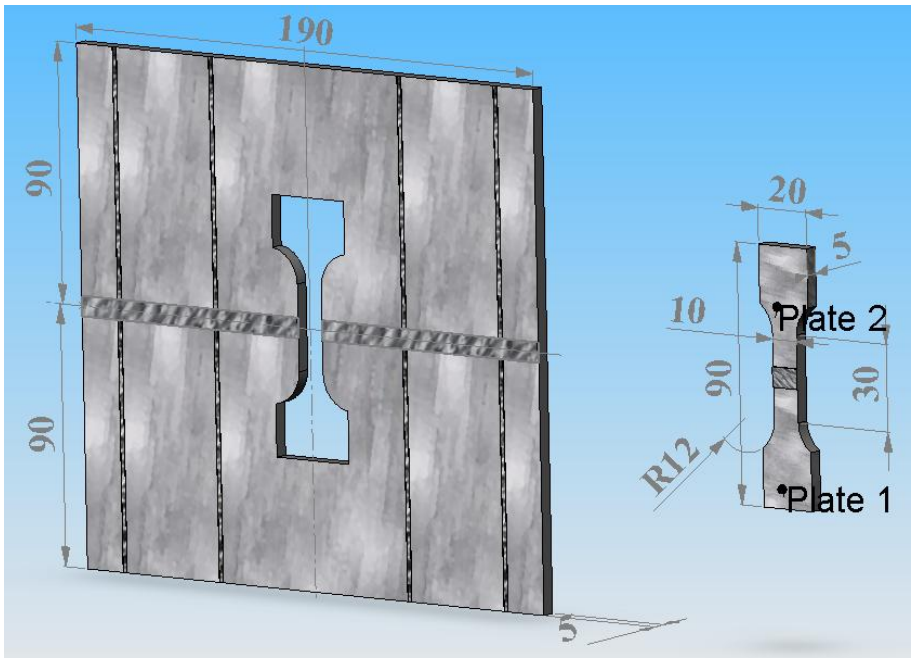


Figure 3.5. Illustration of distribution planning of the specimens on the sheet material

All the tests were conducted to failure and the specimen design respects the standard requirements. The significant rupture surfaces were prepared by standard metallographic techniques and etched with reagent, in order to study the grain structure of the welded zones and to allow optical microscopy characterization. Tensile test samples were prepared for Bakelite processing and also were molded for Bakelite molding. Consist of hardener, accelerator and epoxy resin that solution was prepared and molded. Bakelites that removed from mold were grinded with 400, 600, 800, and 1200 discs and waited in Keller etchant in 2 minutes for each material. Keller etchant was used for 5xxx series aluminum alloys. For optical microscopy, cross sections were polished and etched using a Keller's reagent (nominally 1,5 ml HCl, 2,5 ml HNO_3, 1 ml HF, 95 ml H_2O 5% hydrofluoric acid in diluted water for 180 s at room temperature). After, spaces of the materials were flushed, polished and examined with OM in Faculty of Technical Education at University of Gazi. These polished sections from both the room temperature experiments were examined and compared in an optical metallograph; including the respective FSW zones and the

base metal far removed from the FSW zone. Optical metallography was performed on the weld metal of both welds and on the base metal to compare the grain structure. Metallographic specimens were extracted from the S–T plane of the base metal sheet. All of the weld metal metallography was performed on a plane perpendicular to the welding direction at the weld centerline and mid-thickness.

Tensile tests were performed in order to evaluate the static properties of the welded joints. We have been executed at room temperature using an Instron Type Hydraulic Testing Machine according to the ASTM E 8 standard code. The tensile test sample is shown in Figure 3.6.

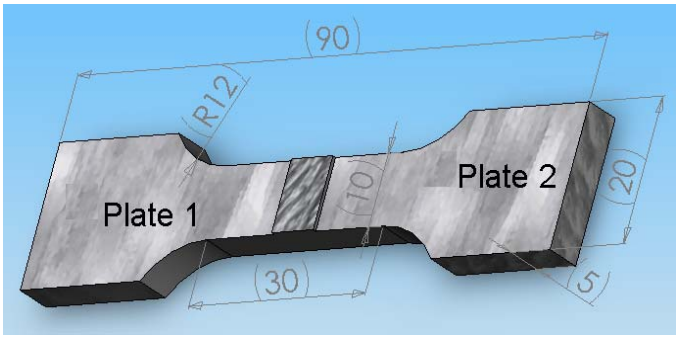


Figure 3.6. Dimension of tensile test piece used in this study

In addition, a scanning electron microscope equipped with field emission gun has been employed to observe the specimens surfaces of fracture either with monotonic and cyclic load; the microscopic morphology and defects of the welded joints and the mechanics involved during tensile failure have been analyzed. Microstructural changes from the weld zone to the unaffected base metal were examined with Optical Microscopy (OM) and Scanning Electron Microscopy (SEM) as shown in Figure 3.7.



Figure 3.7. Scanning Electron Microscopy (SEM) used in this study

The fatigue tests were carried out in a high-frequency fatigue test machine with a capacity of 100 kN load as shown in Figure 3.8. The fatigue specimens were machined perpendicular to the weld line. The weld was transverse to the stress axis in the S–N specimen (cross-weld). The oscillation frequency was in the interval of 110–120 Hz in laboratory air in Industrial Arts Education Faculty of Gazi University. Results of the fatigue tests were examined according to the following equation.

$$W = \frac{b.h^2}{6} \tag{3.1}$$

$$\sigma = \frac{M_e}{W} \tag{3.2}$$

Here,

W = Moment of Inertia [mm^3]

σ = Bending Stress [daN/mm^2]

Me = Bending Moment [daN/mm^2]

b = Width [mm]

h = Height [mm]

Bending fatigue test mechanism gives permission to carry out dynamic fatigue tests DIN50142 with compatible thermoplastics, nonferrous metals and steels. Dynamic and static loads can be applied while mechanism capacity allows. (S-N) Wöhler diagrams and fatigue strength test is used for German Standard DIN50100.

The values resulted of bending fatigue tests and Wöhler curves were logarithmically plotted correspond the greatest cycle values. The tests were evaluated only once for main metals and 10 for each welding joints. In all the tests, cycle number have been consent to be $N_R = 2x10^6$ as boundary cycle number that proposed in literature.



Figure 3.8. High-frequency fatigue test machine used in this study

After fatigue test, broken test samples were investigated to determine the region that fatigue cracking. Fatigue curves of each joint were carried out and plotted. After fatigue test samples were prepared for SEM, the samples were putted

and micro views of the samples were evaluated at Technical Education Faculty of Gazi University.

3.2.1. Microstructure Analysis

In order to analyze joined and base materials; prepared to examine optical microscopy views. The significant rupture surfaces were prepared by standard metallographic techniques and etched with reagent, in order to study the grain structure of the welded zones and to allow optical microscopy characterization. For optical microscopy, cross sections were polished and etched using a Keller's reagent. After, spaces of the materials were flushed, polished and examined with OM in Faculty of Technical Education at University of Gazi. Microstructural changes from the weld zone to the unaffected base metal were examined with Optical Microscopy (OM) and Scanning Electron Microscopy (SEM).

3.2.1.1. Optical Microscopy (OM)

Specimen preparation has become a long established art in the optical microscopy of materials, particularly in the fields of metallurgy and mineralogy. The specimens are prepared ideally representative of the structure of interest and free from damage and contamination. In this study, preparation of specimen has 5 steps and all these steps are illustrated schematically in Figure 3.9. After preparation steps, all specimens investigated with optic microscope and photographed. Preparation and photographing specimens are managed again GAZİ University Mechanical Research Laboratories.

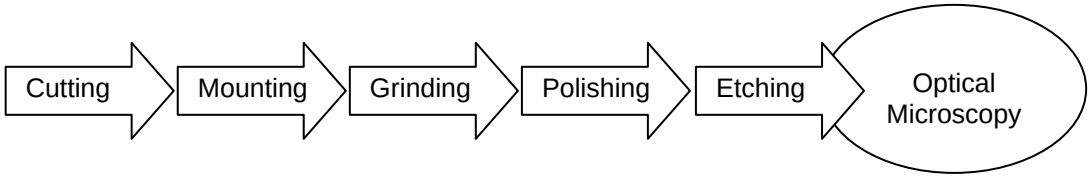


Figure 3.9. Specimen preparation steps

3.2.1.2. Scanning Electron Microscope (SEM)

The Scanning Electron Microscope is commonly used to examine the microstructure of bulk specimens. It is an electron optical instrument which uses a source of electrons to illuminates the specimen. These electrons are accelerated down the column and pass through a combination of electromagnetic lenses and apertures to form a fine probe at the surface of the specimen in the chamber area. Both the column and the chamber are held under vacuum to avoid high voltage discharge and scattering of the electrons along their path by residual gas atoms. A variety of signals are produced as a result of the interaction of the beam with the specimen, which may be collected by appropriated detectors. There is a trade off between good count rate and low noise images and ability to see very fine specimens detail (McCall J.L. 1973).

In order to obtain well researchable images from the parts, compacted specimens were broken and cracked surfaces were investigated. Plastic and elastic particle deformations, effects of cracks can be seen easily with SEM photos.

Scanning Electron Microscopy (SEM) investigations are organized in GAZİ University Mechanical Research Laboratories and Jeol JSM-6060LV Computer Controlled Digital Scanning Electron Microscope is used and shown in Figure 3.7.

4. RESULTS and DISCUSSION

4.1. Mechanical Properties

4.1.1. Evaluation of Hardness and Tensile Test

In the present study, the similar 5186-H111/5186-H111, 5083-O/5083-O, 5083-H111/5083-H111 (Alustar) and dissimilar 5083-O/5186-H111, 5083-O/5083-H111, 5083-H111/5186-H111 aluminum alloys have been successfully joined with the FSW process using 20, 50, 80 mm/min welding speeds.

The Vickers hardness tests were conducted on the welded joints to assess the extent of the HAZ. The procedures employed for hardness testing were in accordance with ASTM Standard E 10–93. The hardness tests were conducted on the static tests specimens, at intervals of 5 mm along the mid-plane of the plates. The variations in the measured hardness values are respectively plotted in Figures 4.1.-Figure 4.6.

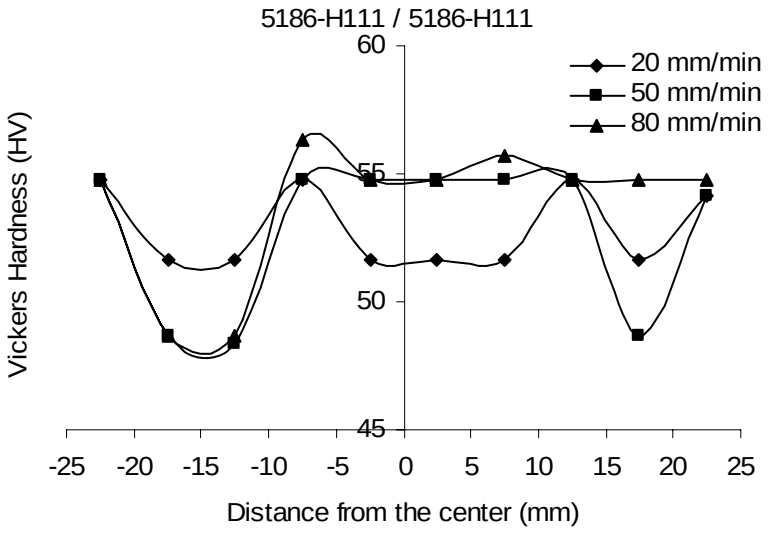


Figure 4.1. The variations in Hardness for 5186-H111 / 5186-H111 weld

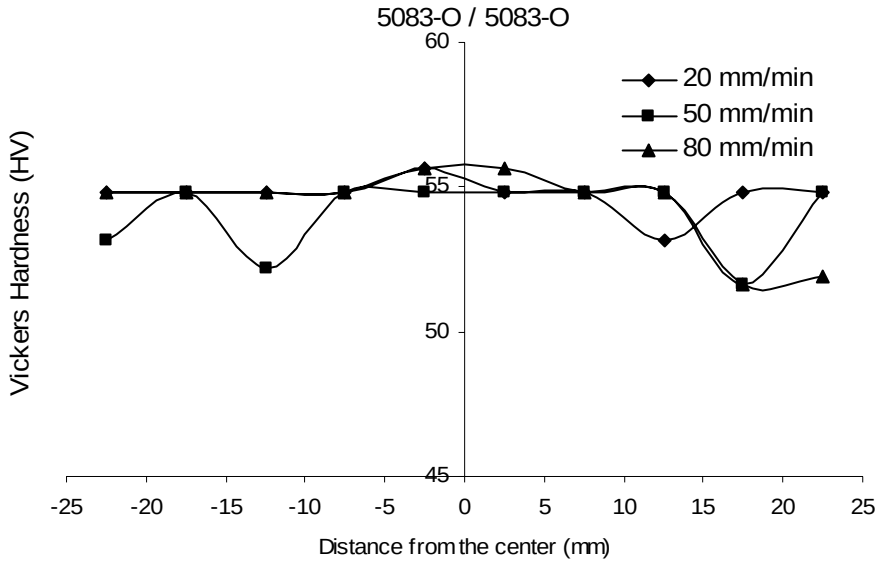


Figure 4.2. The variations in Hardness for 5083-O / 5083-O weld

The micro hardness profile along the FSW is shown in Figure 4.1., in which a value of 52 Hv is reached in the centre weld; the micro hardness profile increases in both the 5186-H111/5186-H111 and then starts to descend after 13 mm from the centre until reaching the hardness corresponding to the welded materials. It can be noticed the welded joint hardness to assume lower values in the HA Zone with respect to both the 5186-H111/5186-H111 welded material, this is in respect of the classical behavior for aluminum alloys welded by FSW.

The joint combination of 5186-H111 and 5083-O has uniform hardness distribution on HAZ. The hardness of the HAZ, in case of 50 and 80 mm/min welding speeds, is uniformly distributed and shows less variation, which ranges from 50 to 55 HV. In contrast, the hardness of the HAZ of 20 mm/min welding speed shows a very scattered value as shown in Figure 4.1. In Figure 4.2., the joint combination of 5083-O and 5083-O has uniform hardness distribution on HAZ for 20, 50 and 80 mm/min welding speeds.

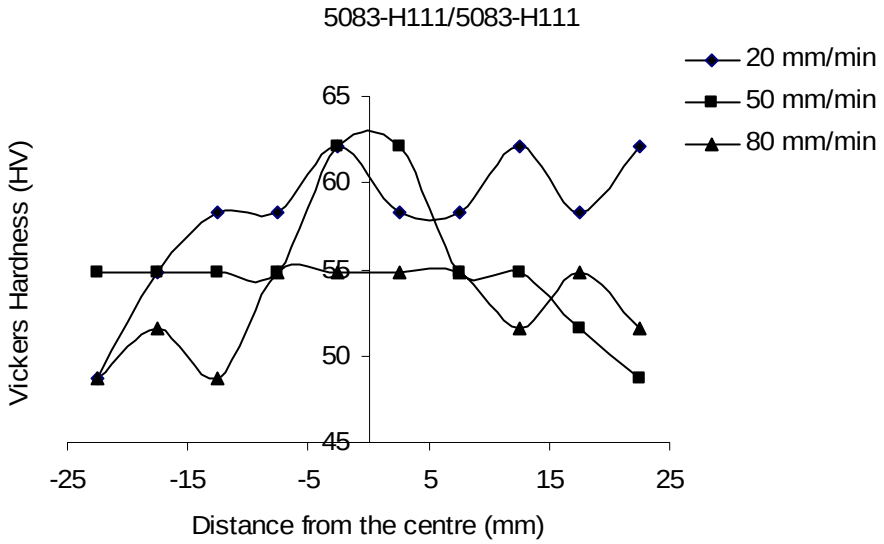


Figure 4.3. The variations in Hardness for 5083-H111/5083-H111 weld

The variations in hardness for 5083-O and 5186-H111 joint combination are shown in Figure 4.4. The hardness of the HAZ shows more uniform values than that of the base materials due to finer and uniformly dispersed Mg_2Si particles. The solid solution hardened Al alloys showed very different behaviors of the hardness distribution in the weld zone. The hardness profile of the weld zone showed roughly homogeneous values and this was mainly governed both dislocation density and the distribution and the size of small particles.

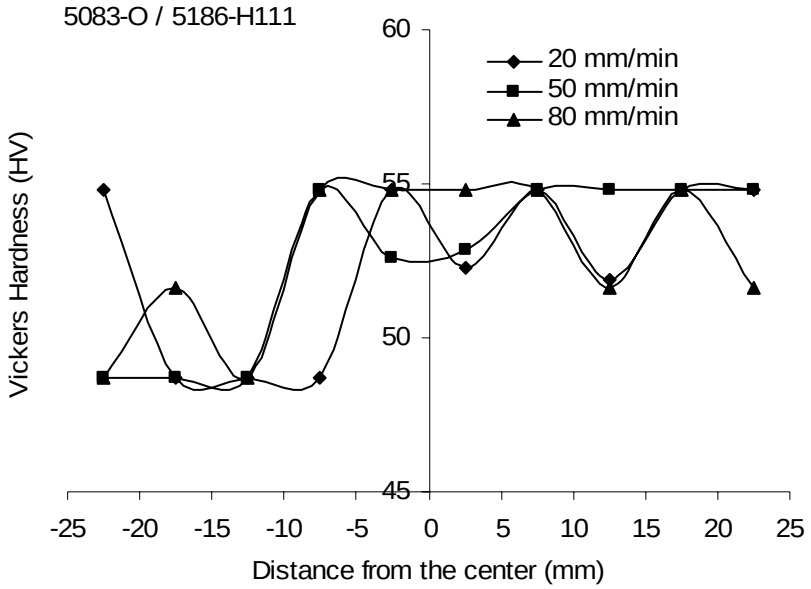


Figure 4.4. The variations in Hardness for 5083-O/5186-H111 weld

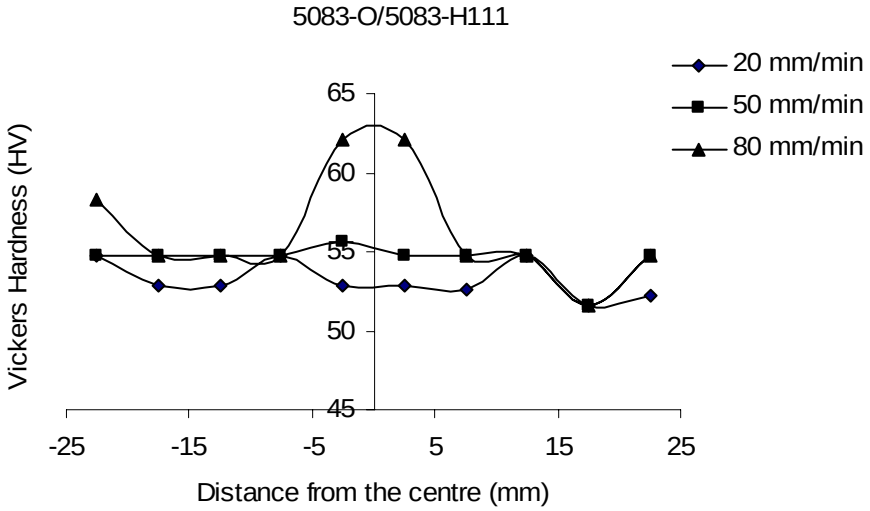


Figure 4.5. The variations in Hardness for 5083-O/5083-H111 weld

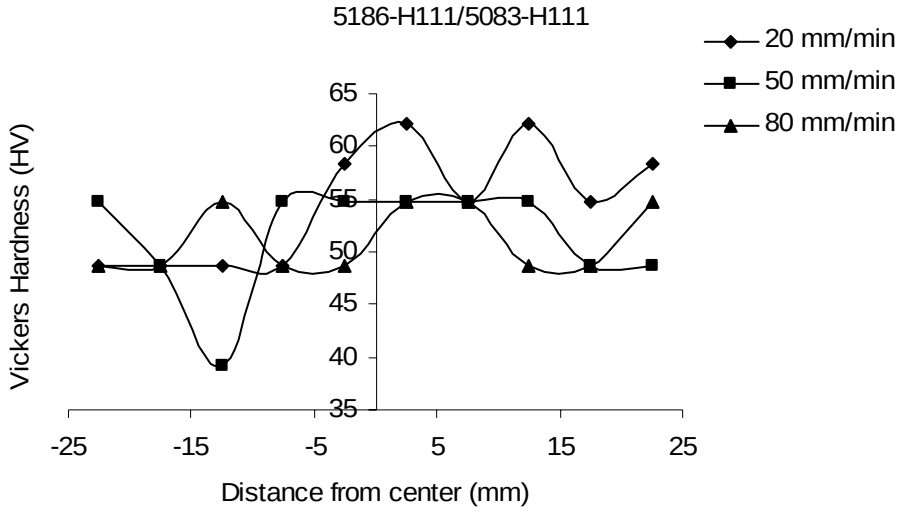


Figure 4.6. The variations in Hardness for 5083-H111/5186-H111 weld

The tensile behavior of the 5186-H111, 5083-O, 5083-H111 and the combinations, 5083-O/5083-O, 5186-H111/5186-H111, 5083-H111/5083-H111 and 5083-O/5186-H111, 5083-O/5083-H111, 5083-H111/5186-H111 material was examined by conducting tensile tests on specimens of each type. In hardness test results, it is realized that 80 mm/min welding speed is selected for optimum welding speed. Because of this, mechanical and microstructural evaluations are made with 80 mm/min welding speed test samples. Table 4.1. shows the average tensile test results with each joint condition. The strengths of the HAZ of similar 5083-O FSW joint showed 281 MPa for ultimate tensile strength (UTS) and 153 MPa for yield strength (YS), which were lower strength than that of 5083-O alloy base metal. The strengths of the HAZ of similar 5186-H111 FSW joint showed 276 MPa for Ultimate Tensile Strength (UTS) and 156 MPa for Yield Strength (YS), which were approximately the same of 5083-O alloy base metal. Figure 4.7.-4.9. show the tensile stress strain curves of FSW joints and Figure 4.10. shows the stress strain curves of base, similar, and dissimilar joints, respectively.

Table 4.1. Ultimate Tensile Stress (UTS) and Yield Stress (YS) diagrams of base, similar joined and dissimilar joined materials

	Base Materials		
Average	5186-H111	5083-O	5083-H111
UTS (N/mm^2)	298	302	367
YS (N/mm^2)	91	114	131
	Similar Joined Materials		
	5186-H111/ 5186-H111	5083-O/ 5083-O	5083-H111/ 5083-H111
UTS (N/mm^2)	256	225	276
YS (N/mm^2)	185	156	110
	Dissimilar Joined Materials		
	5083-O/ 5186-H111	5083-O/ 5083-H111	5186-H111/ 5083-H111
UTS (N/mm^2)	193	248	195
YS (N/mm^2)	111	202	80

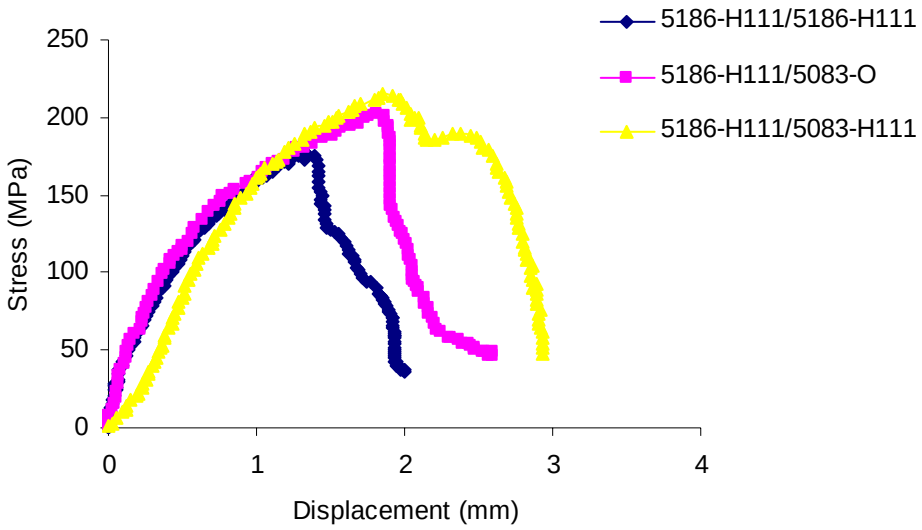


Figure 4.7. Tensile Stress Curves of FS Welded 5186-H111/5186-H111, 5186-H111/5083-O, 5186-H111/5083-H111 Joints

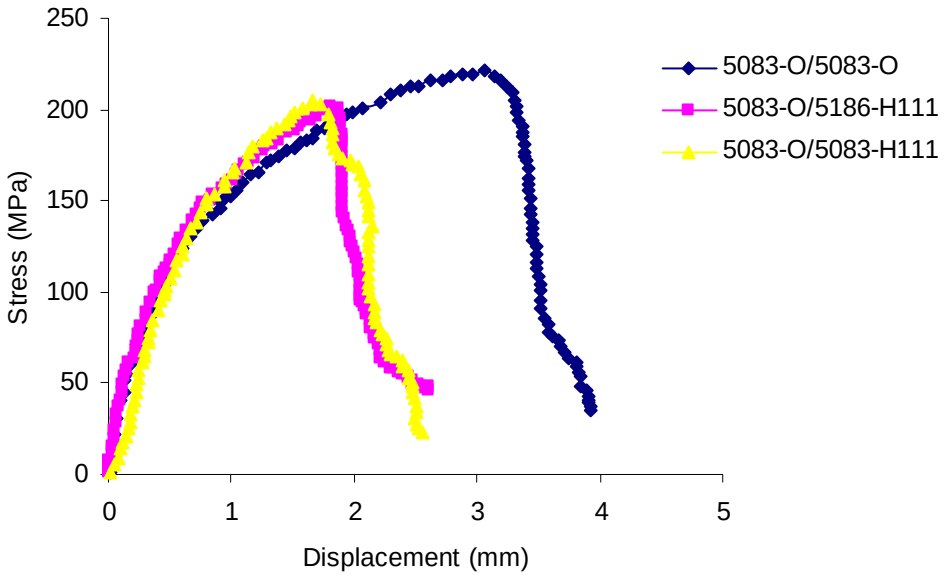


Figure 4.8. Tensile Stress Curves of FS Welded 5083-O/5083-O, 5083-O/5186-H111, 5083-O/5083-H111 Joints

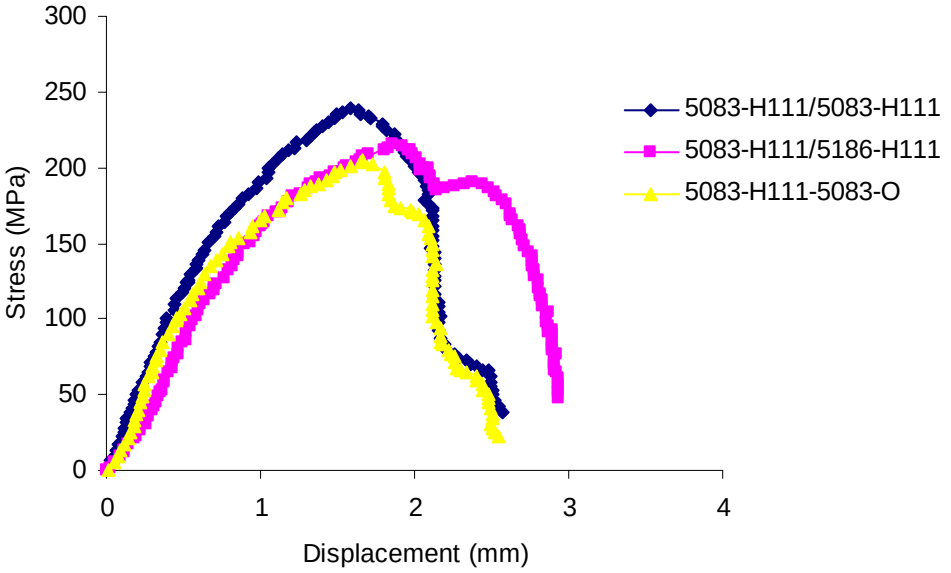


Figure 4.9. Tensile Stress Curves of FS Welded 5083-H111/5083-H111, 5083-H111/5186-H111, 5083-H111/5083-O Joints

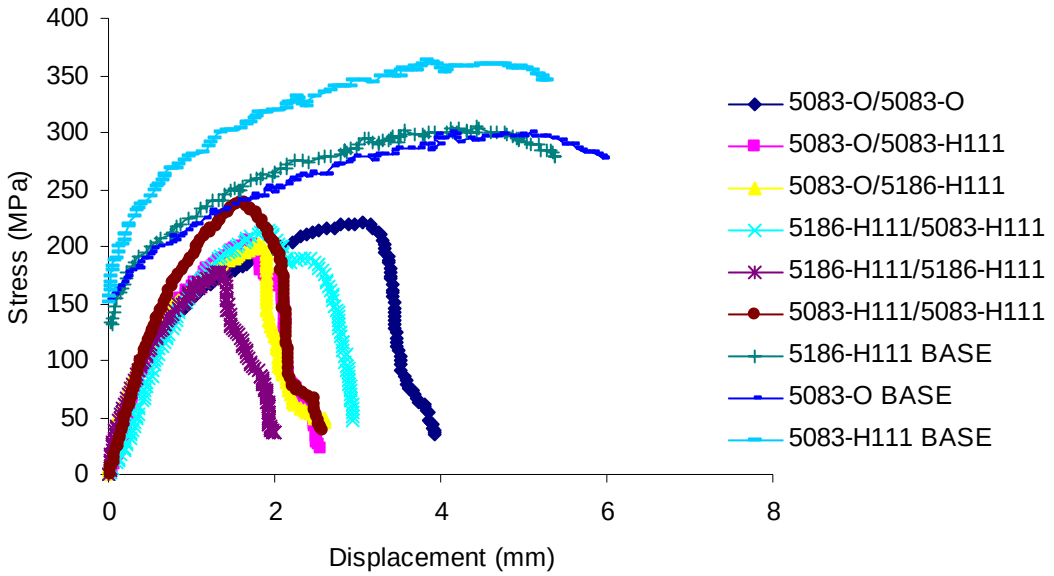


Figure 4.10. Stress Curves Comparison of FS Welded Joints

4.1.2. Evaluation of Fatigue Test

All the tests were conducted to failure and the specimen design respects the standard requirements. Successively, the significant rupture surfaces were prepared by standard metallographic techniques and etched with Keller's reagent, in order to study the grain structure of the welded zones and to allow optical microscopy characterization.

Fatigue tests were conducted in the axial loading mode, which is more severe than bending. The fatigue test machine including clamping of the specimen used in this investigation is seen Figure 3.8. A sinusoidal load-time function was used. The frequency was f=20 s^{-1} two stress ratios were investigated with the unnotched specimens (Kt = 1.0) under fully reversed loading ($\boldsymbol{R}$= $\sigma_{min}/\sigma_{max}$ = -1) using 9 specimens for the determination of each S-N curve, in Figure 4.11.-4.19. Average stresses in the interval of 60–190 MPa were tested. The Woehler curves, presented in terms of nominal stress amplitude σ_{an} and cycles to rupture N_R, were statically evaluated for the probabilities of 10, 50, 90 of a logarithmic Gaussian distribution.

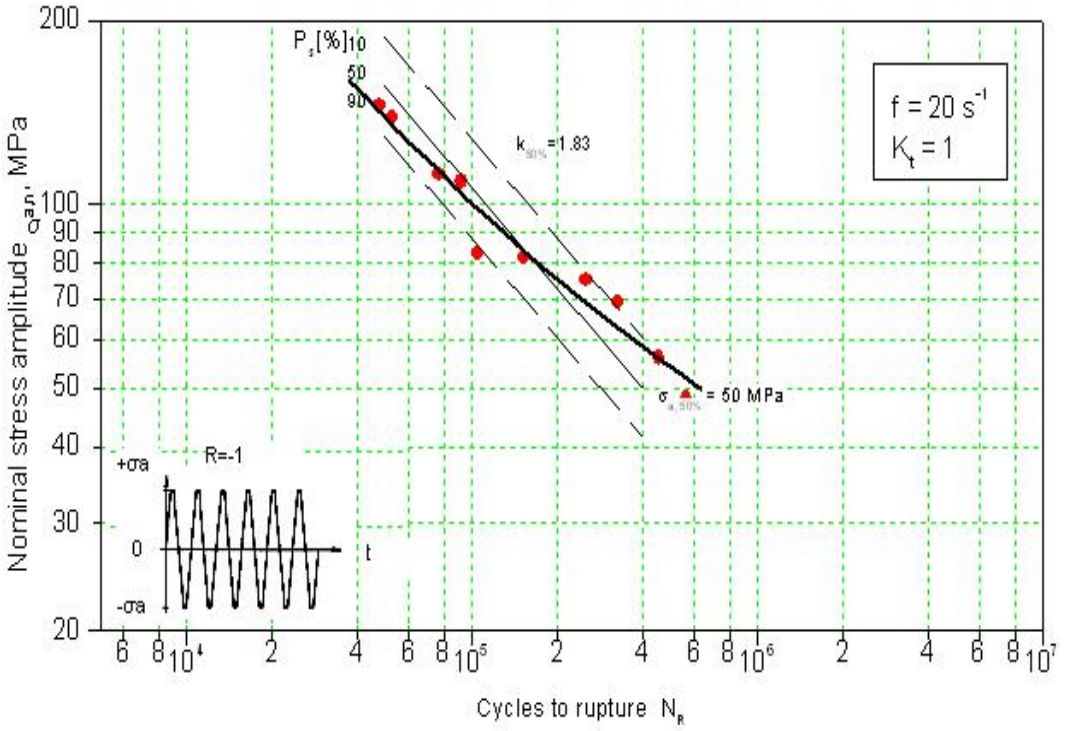


Figure 4.11. S-N Curve of FS Welded 5186-H111 Base

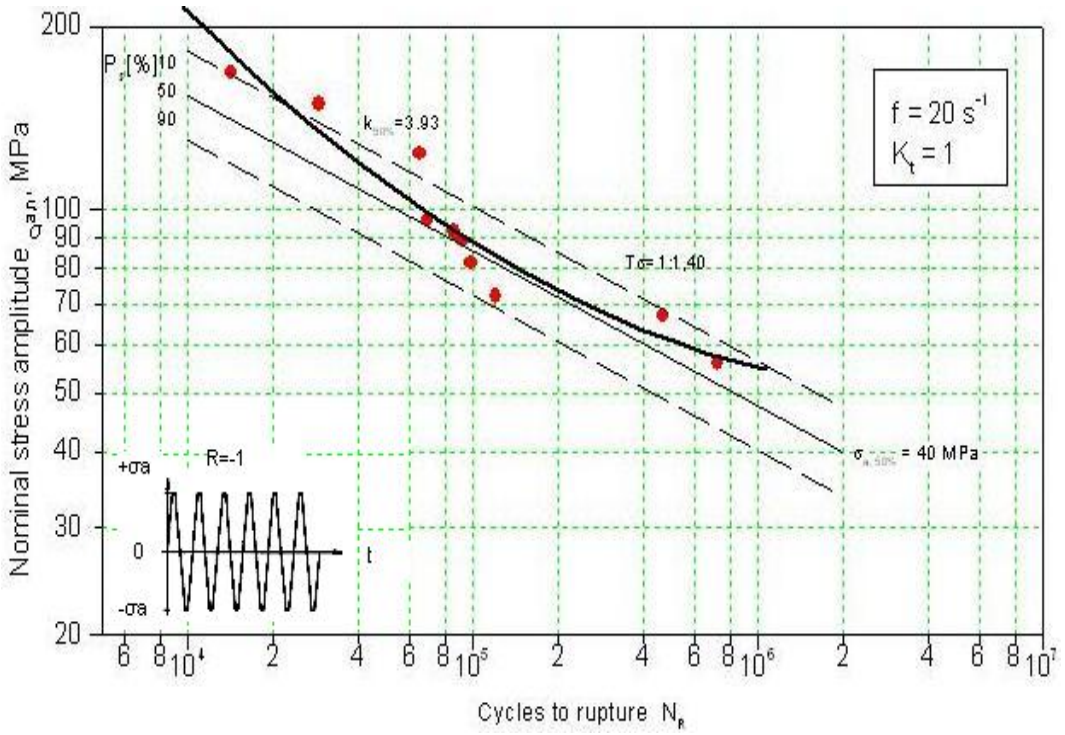


Figure 4.12. S-N Curve of FS Welded 5083-O Base

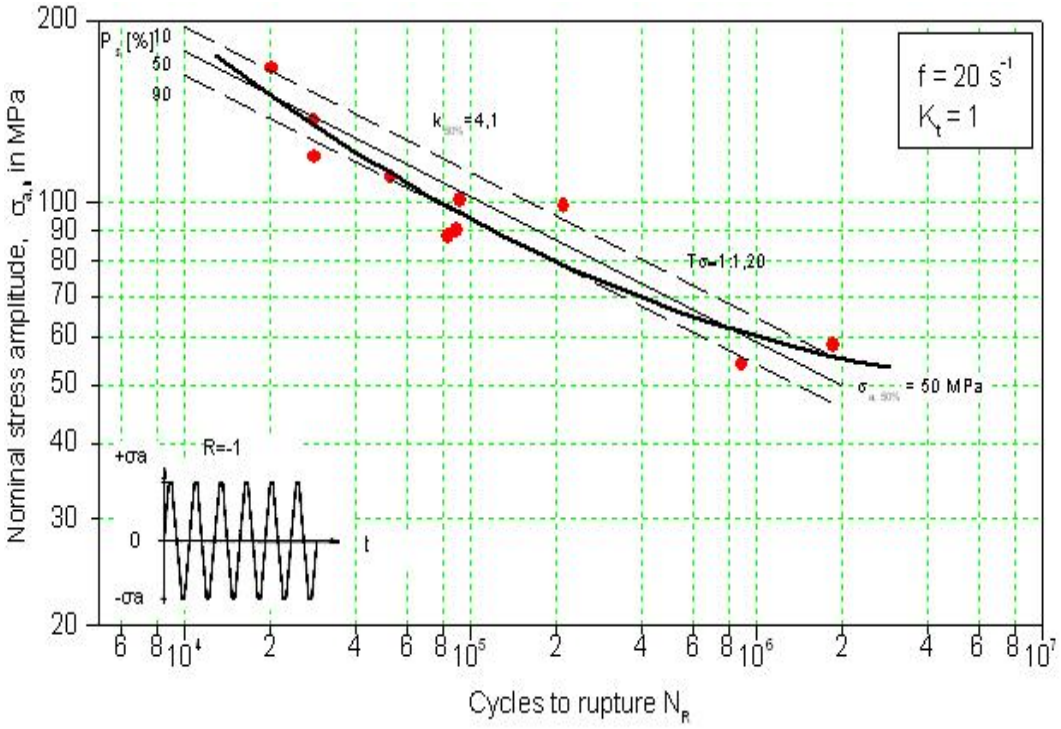


Figure 4.13. S-N Curve of FS Welded 5083-H111 Base

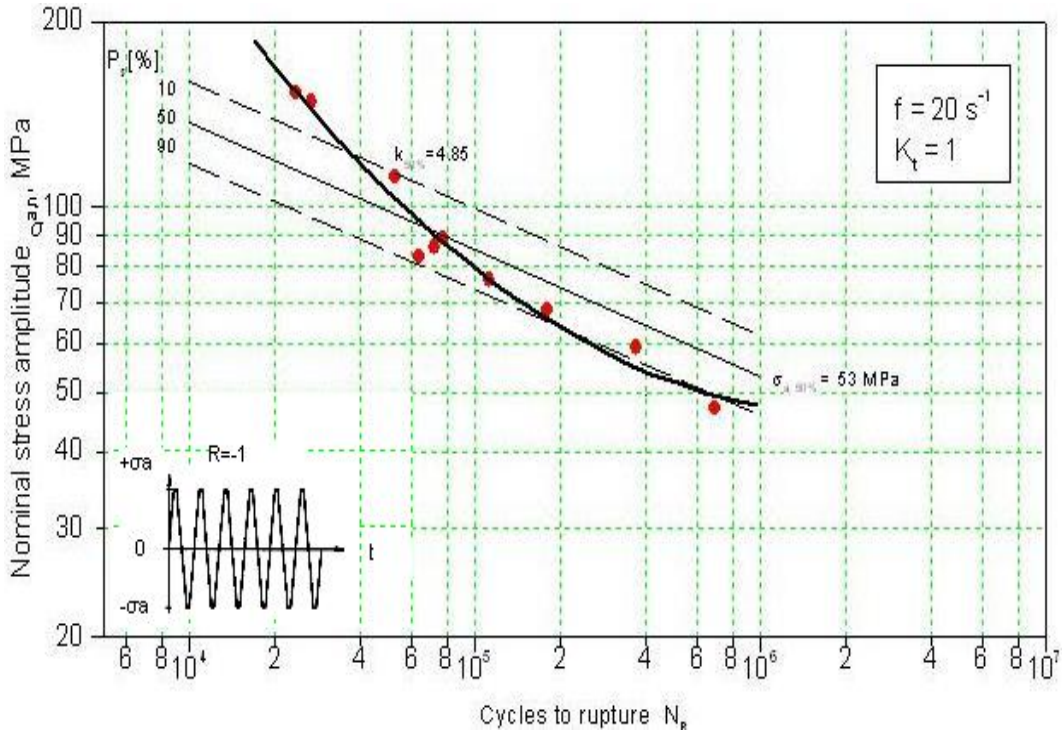


Figure 4.14. S-N Curve of FS Welded 5083-O/5083-O Joint

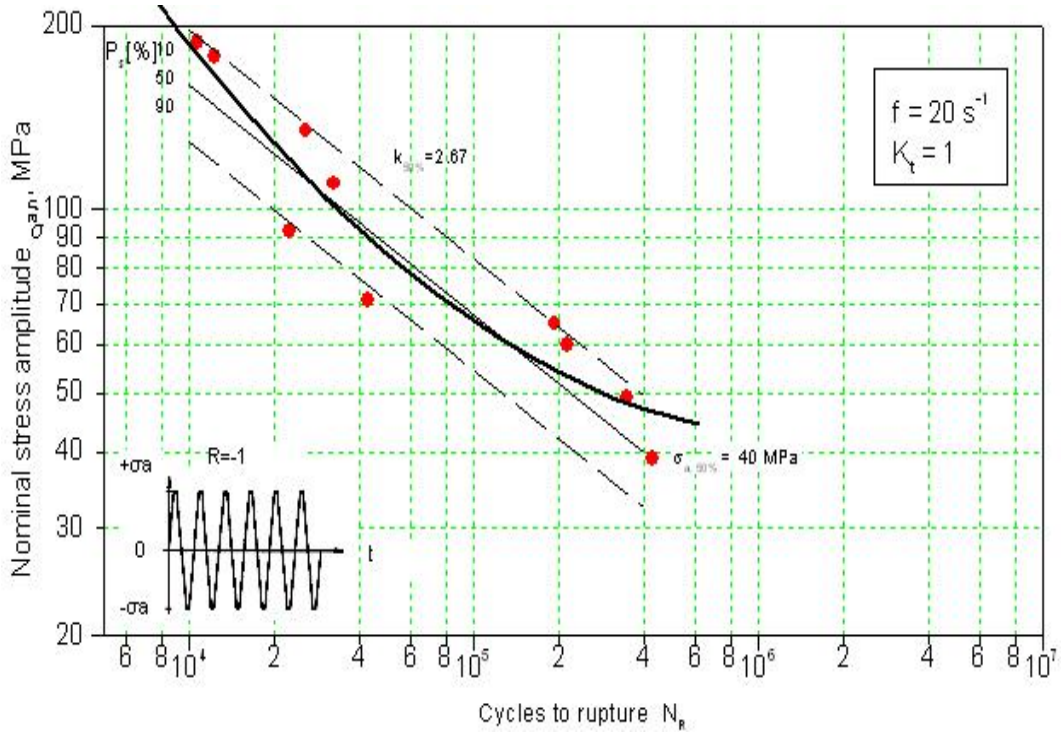


Figure 4.15. S-N Curve of FS Welded 5186-H111/5186-H111 Joint

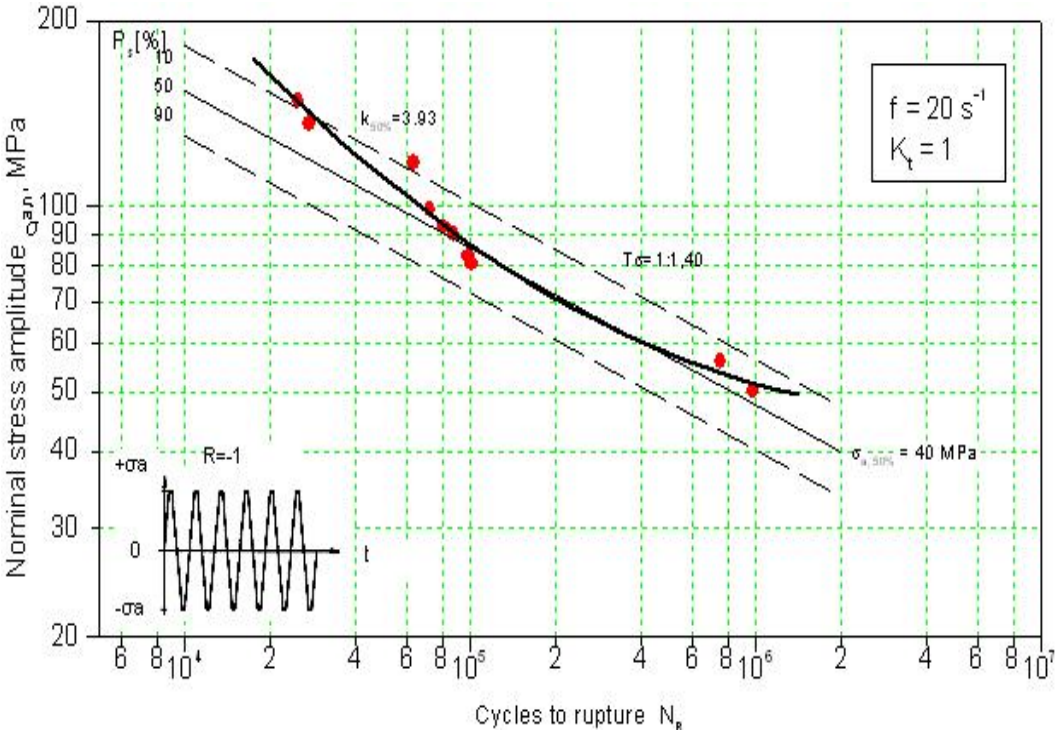


Figure 4.16. S-N Curve of FS Welded 5083-H111/5083-H111 Joint

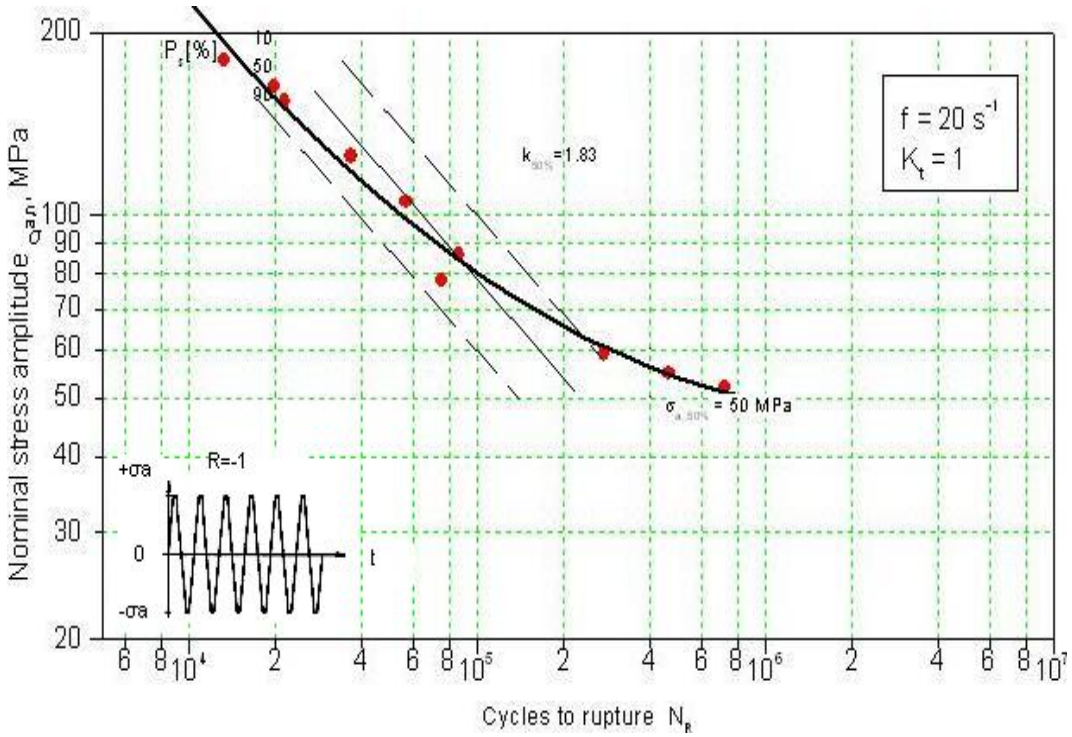


Figure 4.17. S-N Curve of FS Welded 5083-O/5186-H111 Joint

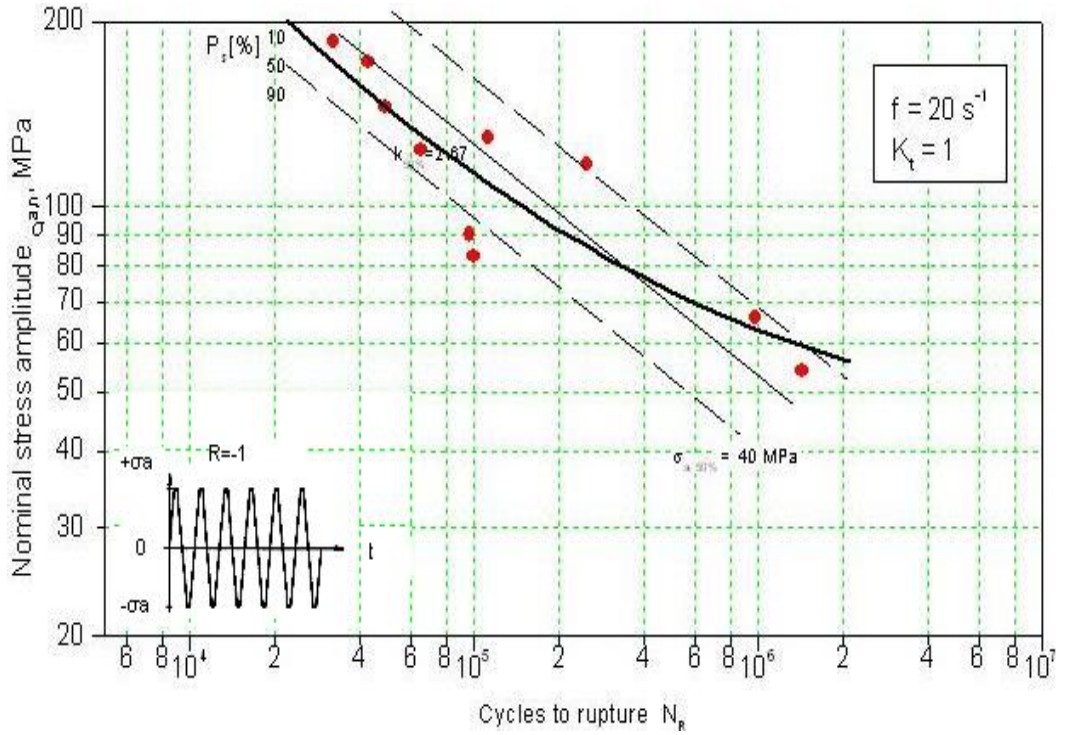


Figure 4.18. S-N Curve of FS Welded 5083-O/5083-H111 Joint

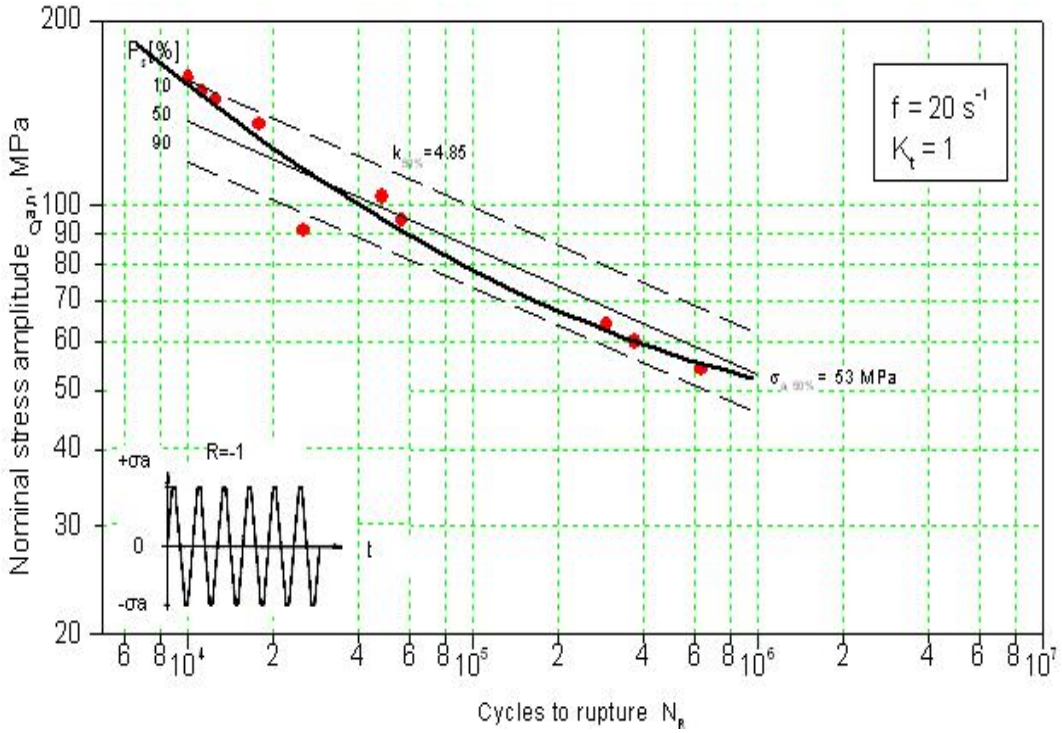


Figure 4.19. S-N Curve of FS Welded 5186-H111/5083-H111 Joint

4.2. Metallurgical Evaluation

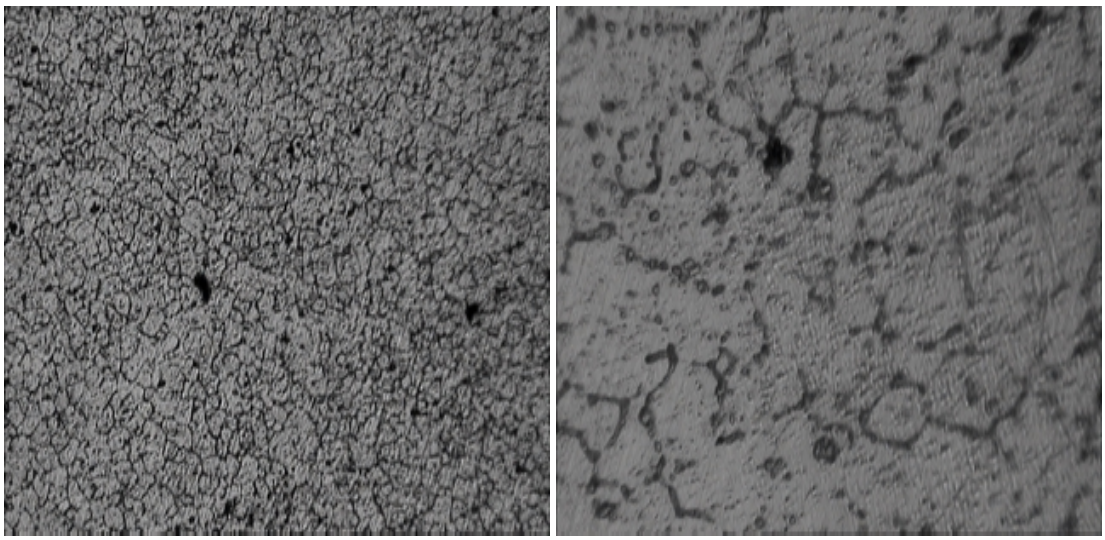
4.2.1. Optical Microscope (OM)

Optical microscopy observations have been done on the FS welded 5186-H111/5186-H111, 5083-O/5083-O, 5083-H111/5083-H111 and dissimilar 5083-O/5186-H111, 5083-O/5083-H111, 5083-H111/5186-H111 on the base and near the weld zone.

Polished and etched Al parts photographed to investigate for this study. Optical photographs are taken in 10X and 40X scales from optic microscope with video capture. General pore structures on the surface can be seen clearly with 40X scaled photographs. Structure of FS welded aluminum base and joint materials are shown in Figure 4.20.-4.28.

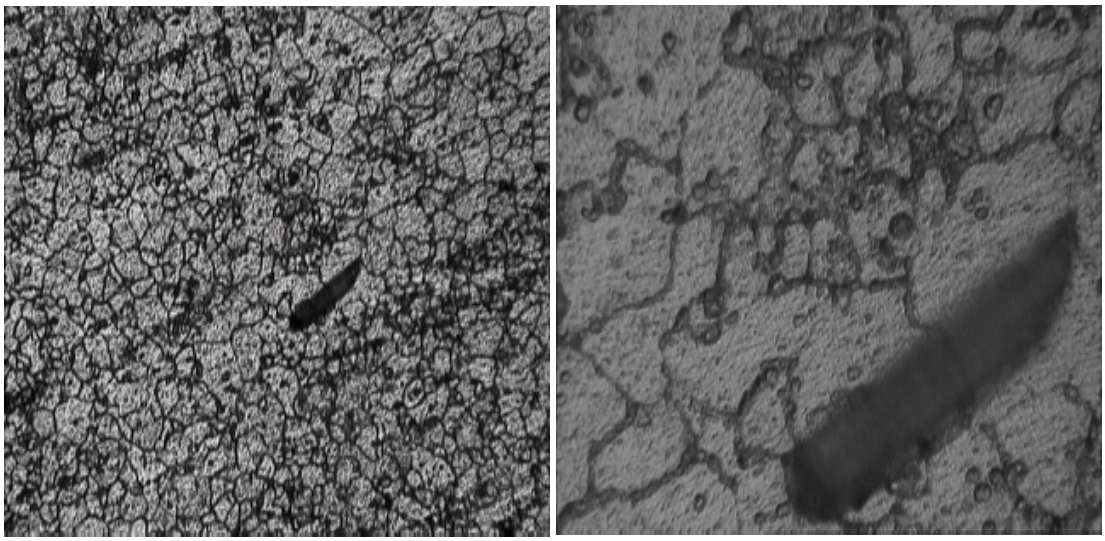
As seen in the Figures, structures are become homogenous and pore. Also grain boundaries appeared notably in Figure 4.20.b, Figure 4.21.b, Figure 4.22.b.

Grain necks are constituted notably and homogeneous structure obtained, smooth and less porosity surface can be seen in Figure 4.21. Shrinkage of the pores initiated with 40X in Figure 4.22.



(a) (b)

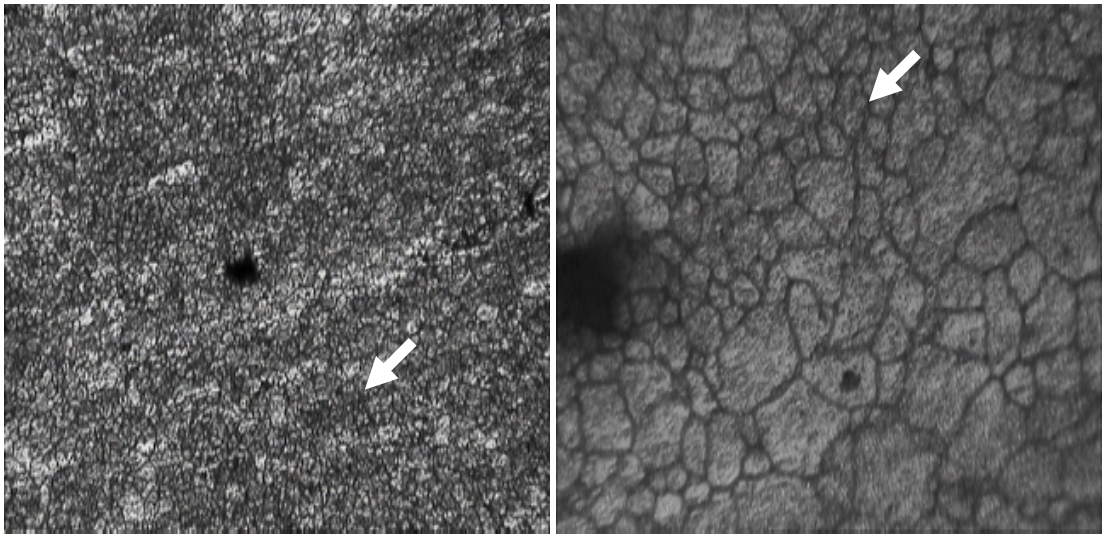
Figure 4.20. Optical Microstructural Analysis of FS Welded 5186-H111 Base (a:10X-b:40X)



(a) (b)

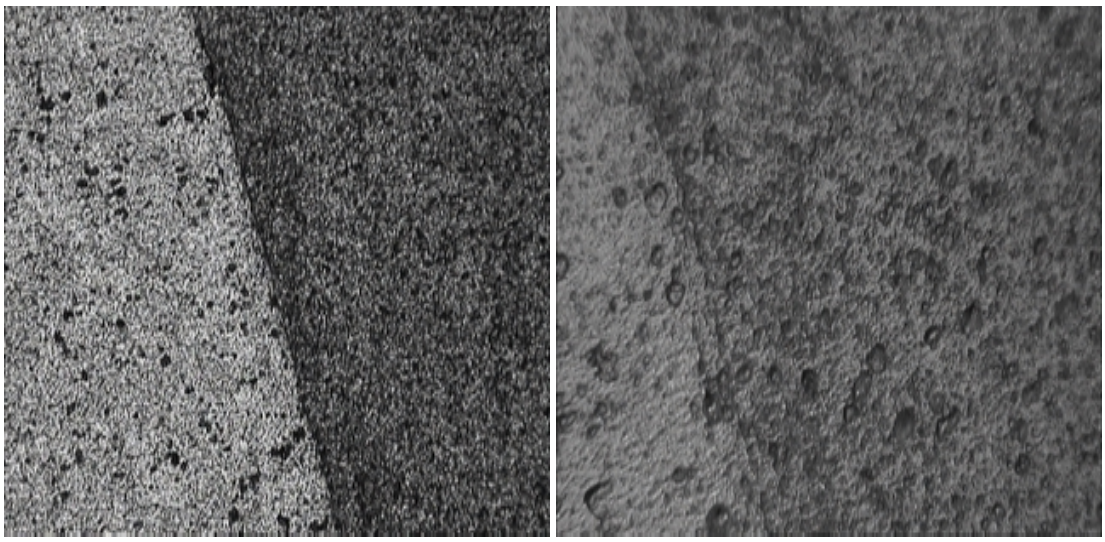
Figure 4.21. Optical Microstructural Analysis of FS Welded 5083-O Base (a:10X-b:40X)

Figure 4.22.a. and Figure 4.22.b. represents the 'nugget' zone at a distance of 2 mm from the weld centre at the 5083-H111 base, which consists of fine and equiaxed grains (Salem H.G., 2003). The higher temperatures and severe plastic deformations result in remarkable smaller grains compared to the base metal, according to all the FSW literature data for aluminum alloys; the initial elongated grains of the parent materials are mechanically converted to a new equiaxed fine grain structure. At higher magnifications, the optical micrographs show extremely fine and equiaxed grains in the recrystallized zones



(a) (b)

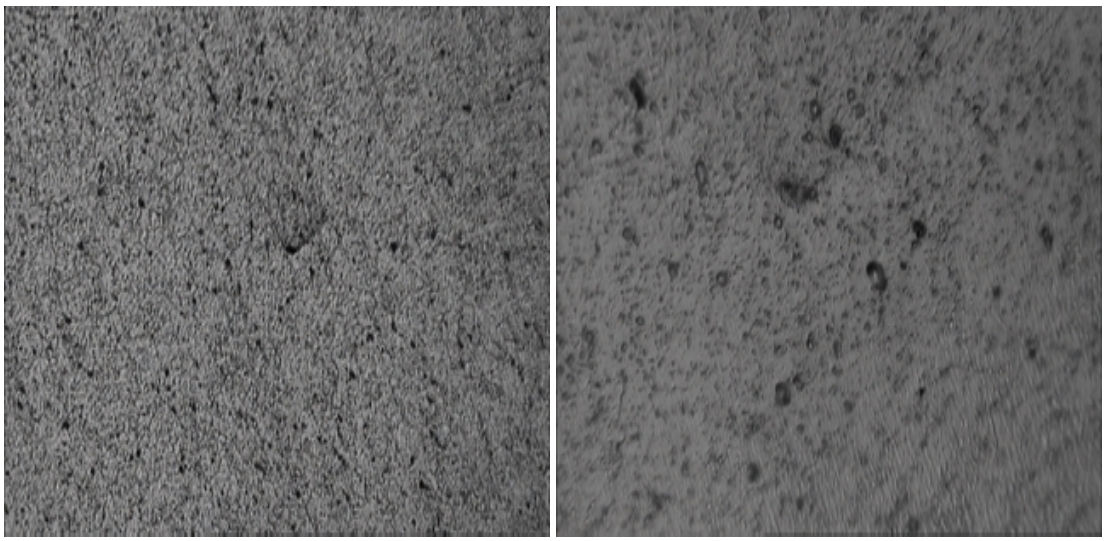
Figure 4.22. Optical Microstructural Analysis of FS Welded 5083-H111 Base (a:10X-b:40X)



(a) (b)

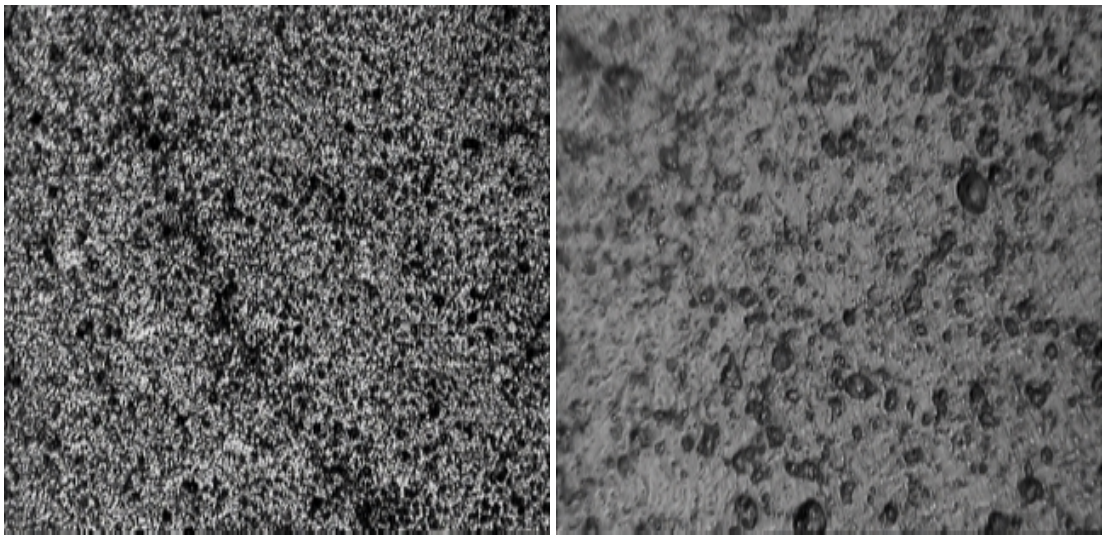
Figure 4.23. Optical Microstructural Analysis of FS Welded 5083-O/5083-O Joint (a:10X-b:40X)

Figure 4.24. shows typical microstructure in the nugget of a FSW weld on a plane normal to the weld direction. This region corresponds to the Heat Affected Zone, where the hardness is low with respect to the base metal.



(a) (b)

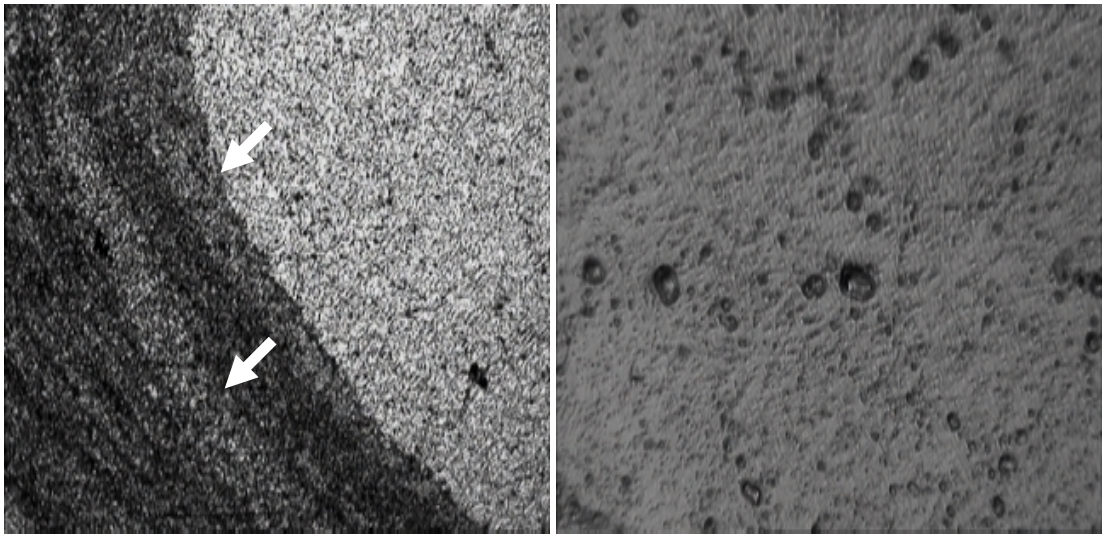
Figure 4.24. Optical Microstructural Analysis of FS Welded 5186-H111/5186-H111 Joint (a:10X-b:40X)



(a) (b)

Figure 4.25. Optical Microstructural Analysis of FS Welded 5083-H111/5083-H111 Joint (a:10X-b:40X)

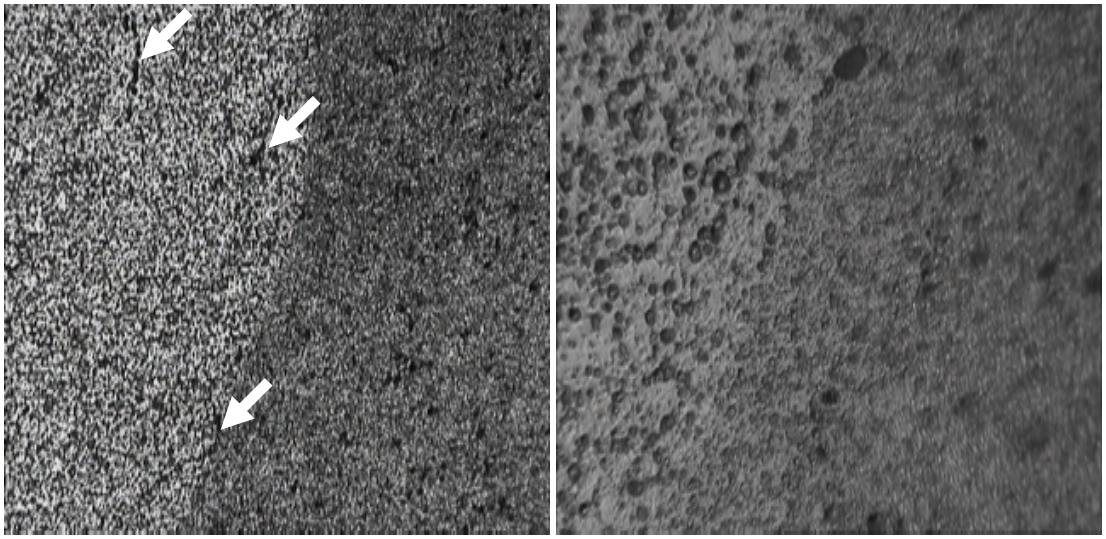
The FSW process applied on dissimilar 5083-O and 5186-H111 aluminum alloys revealed the classical formation of the elliptical ‘onion’ structure in the centre weld; this is confirmed by the microstructure with fine recrystallized grains. The Thermo Mechanical Affected Zone (TMAZ) is also distinguished through optical microscopy. Figure 4.26.a shows cross section of the welded specimen: particular of the nugget zone and base material interface.



(a) (b)

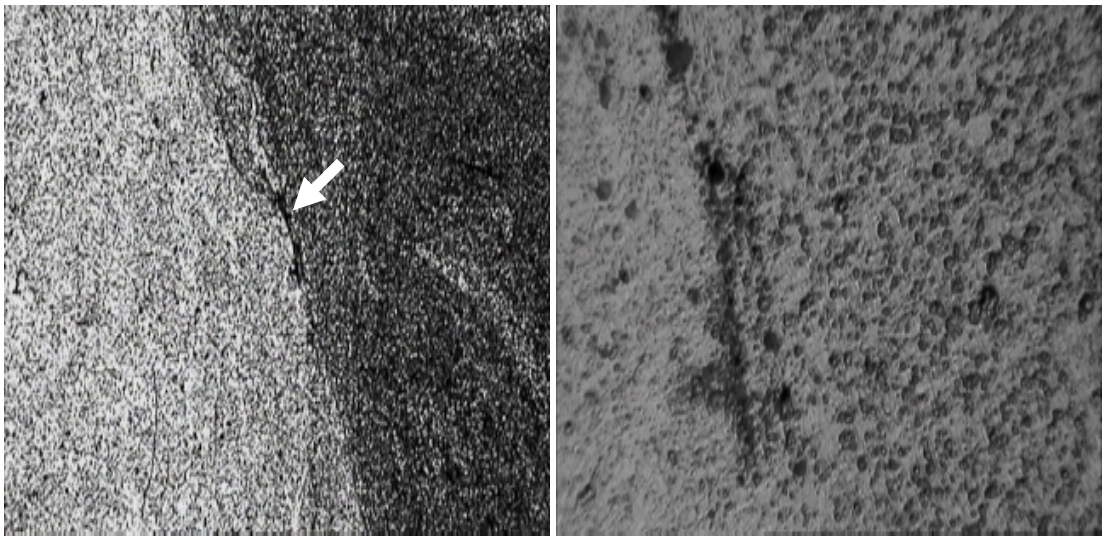
Figure 4.26. Optical Microstructural Analysis of FS Welded 5083-O/5186-H111 Joint (a:10X-b:40X)

Figure 4.26.a., 4.27.a and 4.28.a. show the tip of the crack, which is progressing from left to right. It can be seen that the crack is preceded by a large number of voids that formed all the way along the remains of the weld line down to the root of the weld.



(a) (b)

Figure 4.27. Optical Microstructural Analysis of FS Welded 5083-O/5083-H111 Joint (a:10X-b:40X)



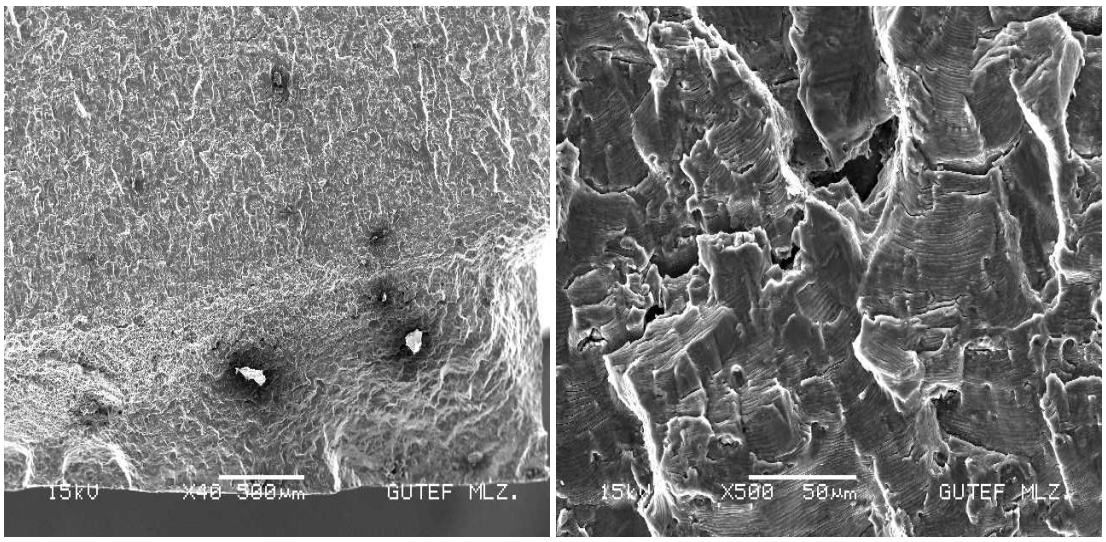
(a) (b)

Figure 4.28. Optical Microstructural Analysis of FS Welded 5186-H111/5083-H111 Joint (a:10X-b:40X)

4.2.2. Scanning Electron Microscope (SEM)

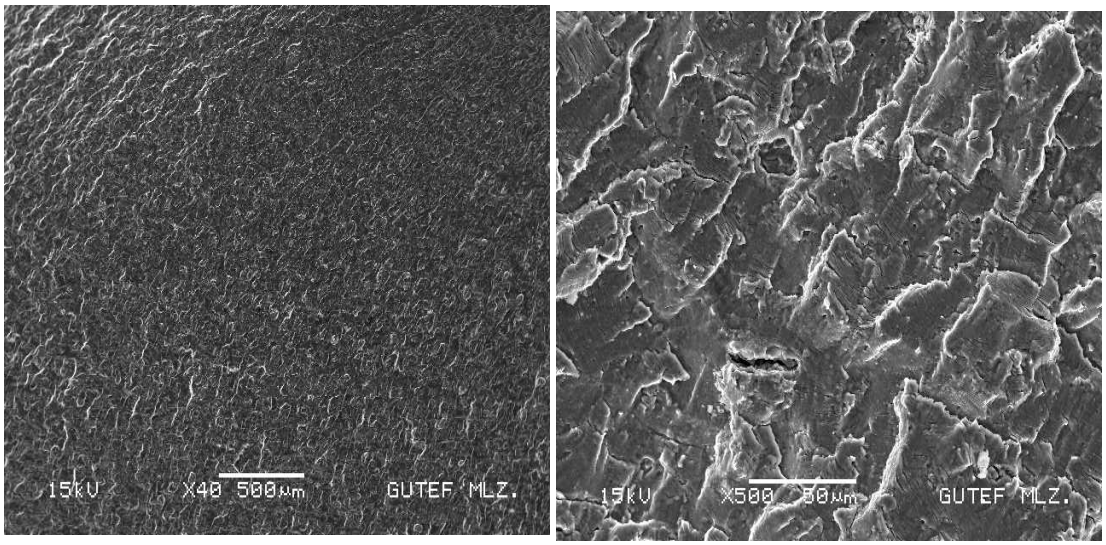
Scanning Electron Microscope (SEM) photographs are taken at Faculty of Technical Education at University of Gazi with Jeol JSM-6060LV Computer Controlled Digital Scanning Electron Microscope test machine. 40X and 100X scales are used for fatigue test specimens in this investigation.

FS welded aluminum base and joint specimens are researched as shown in Figure 4.29-4.40. and it is enough to show the structure clearly.



(a) (b)

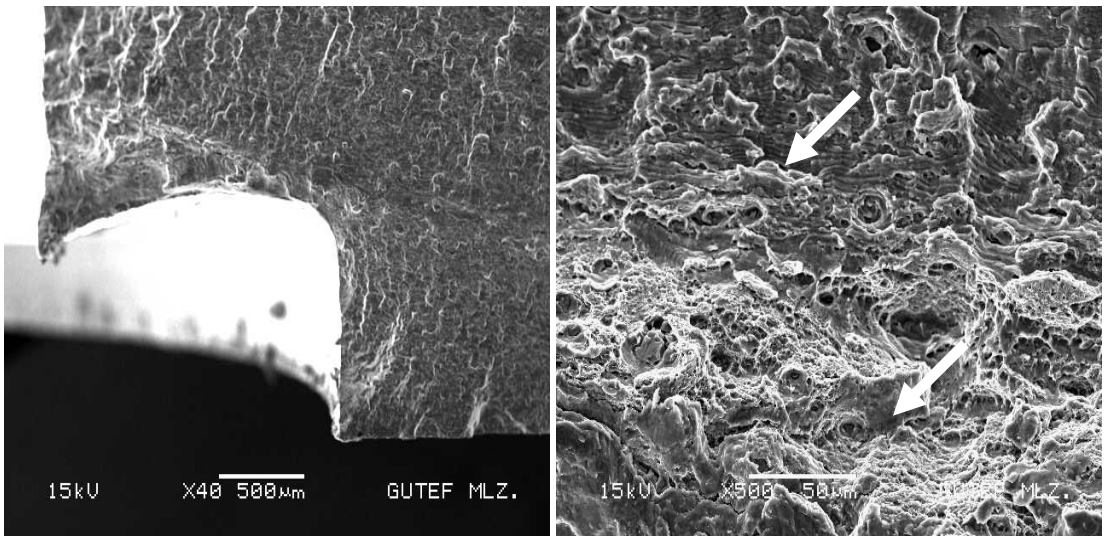
Figure 4.29. SEM Views of Fracture Surfaces of FS Welded 5186-H111 Base (a:40X, 500µm-b:500X, 50µm)



(a) (b)

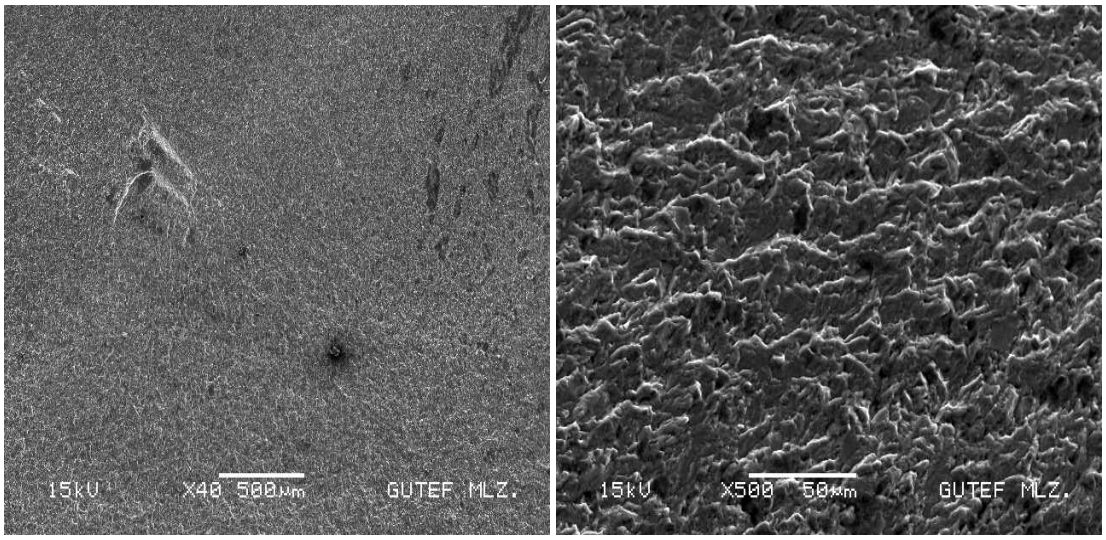
Figure 4.30. SEM Views of Fracture Surfaces of FS Welded 5083-O Base (a:40X, 500µm-b:500X, 50µm)

Samples of FS welded 5083-H111/5083-H111 and 5083-H111 base plate were not notched in the parent material, and the weld nugget region and then fractured. The fracture surfaces were examined using scanning electron microscopy. Both the weld nugget and the parent material failed in a ductile manner by the microvoid coalescence mechanism as shown in Figure 4.31.b. and Figure 4.34.b. However, there was an absence of relatively large microvoids in the weld nugget sample and this may be a consequence of the break up of the primary constituent particles during stir welding.



(a) (b)

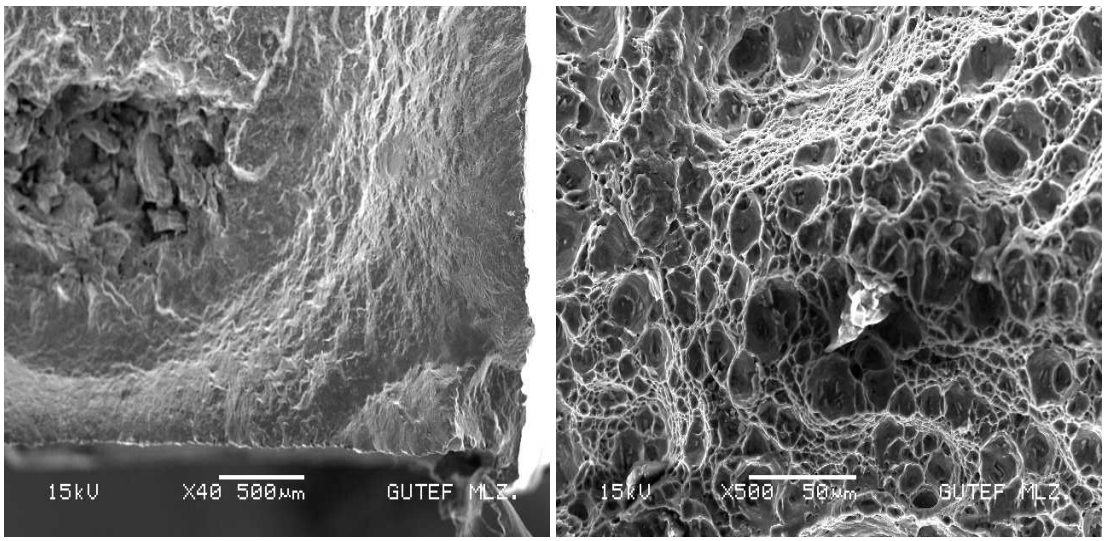
Figure 4.31. SEM Views of Fracture Surfaces of FS Welded 5083-H111 Base (a:40X, 500µm-b:500X, 50µm)



(a) (b)

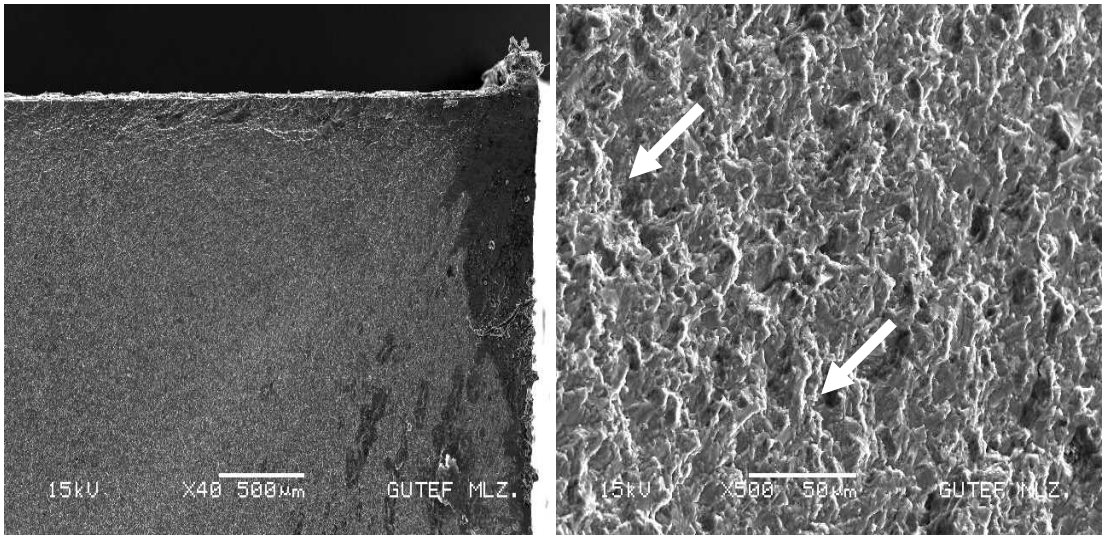
Figure 4.32. SEM Views of Fracture Surfaces of FS Welded 5083-O/5083-O Joint (a:40X, 500µm-b:500X, 50µm)

The fracture face appearance changed drastically with location across the weld. Figure 4.33.b. shows the fracture surface found in the nugget region. This was relatively smooth and flat with local changes of crack plane. In contrast, Figure 4.38.b. shows the fracture surface from a crack parallel to the weld.



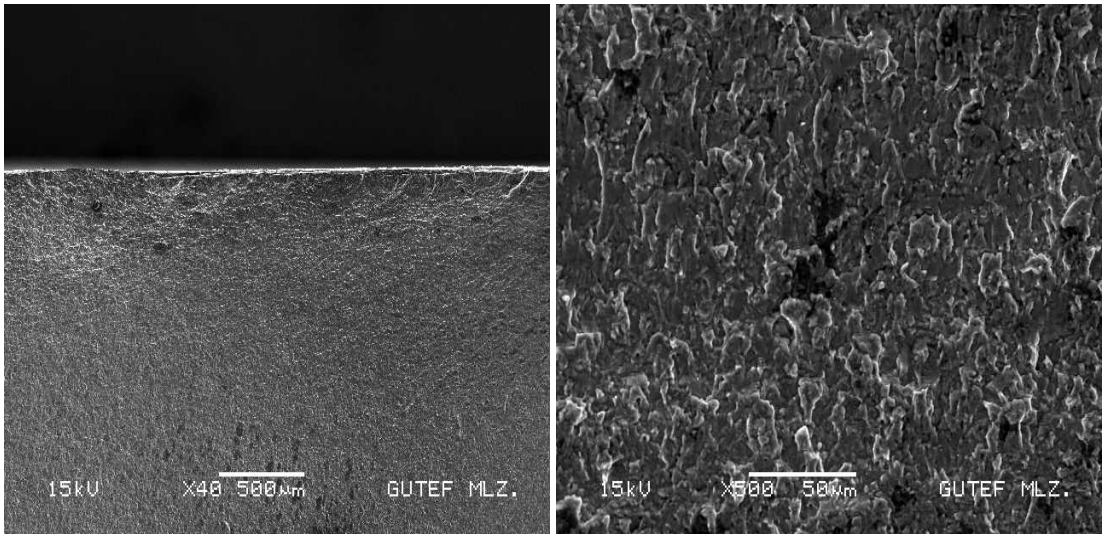
(a) (b)

Figure 4.33. SEM Views of Fracture Surfaces of FS Welded 5186-H111/5186-H111 Joint (a:40X, 500µm-b:500X, 50µm)



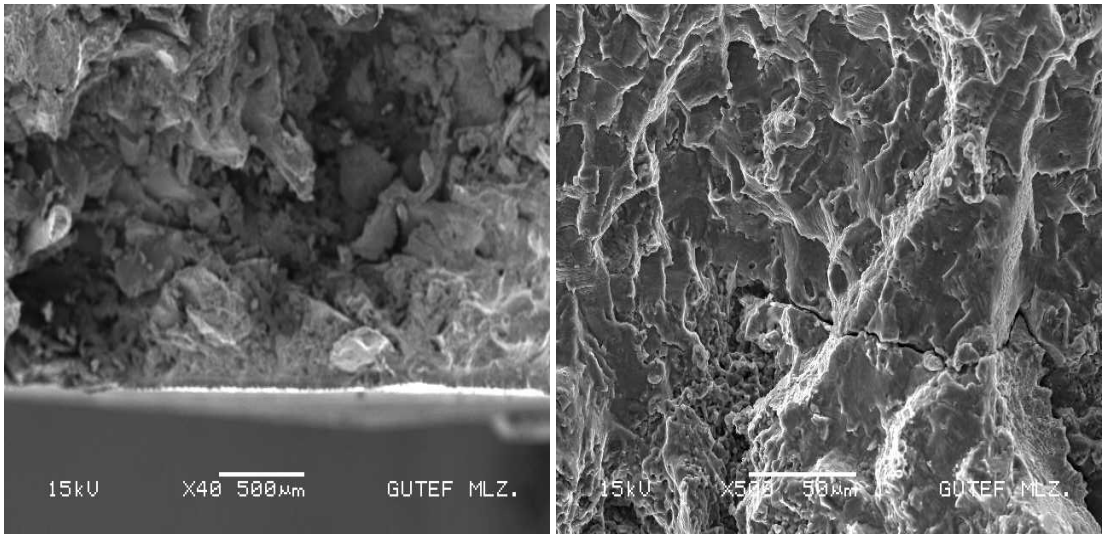
(a) (b)

Figure 4.34. SEM Views of Fracture Surfaces of FS Welded 5083-H111/5083-H111 Joint (a:40X, 500µm-b:500X, 50µm)



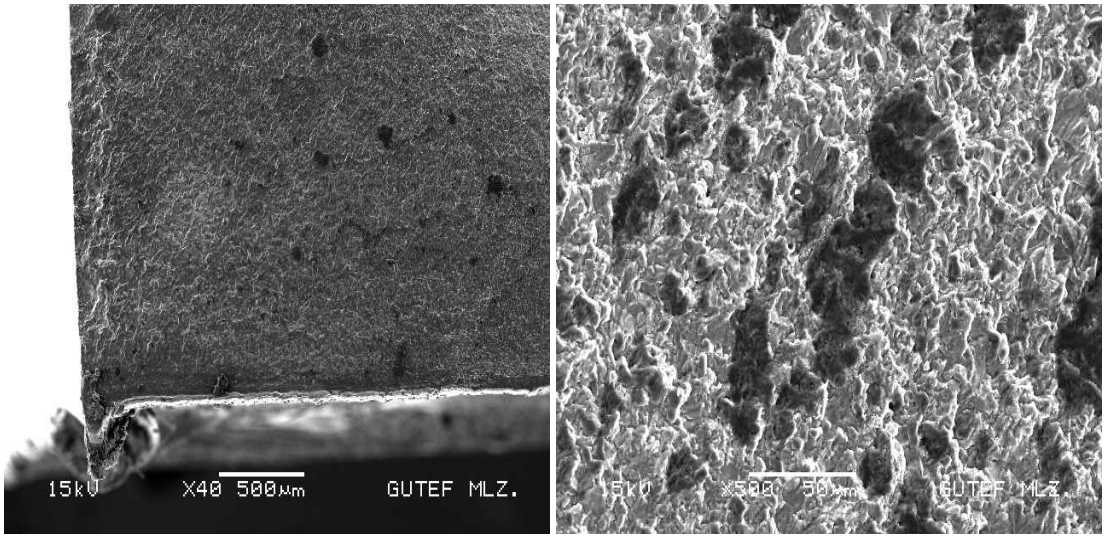
(a) (b)

Figure 4.35. SEM Views of Fracture Surfaces of 5083-O Side of FS Welded 5083-O/5186-H111 Joint (a:40X, 500µm-b:500X, 50µm)



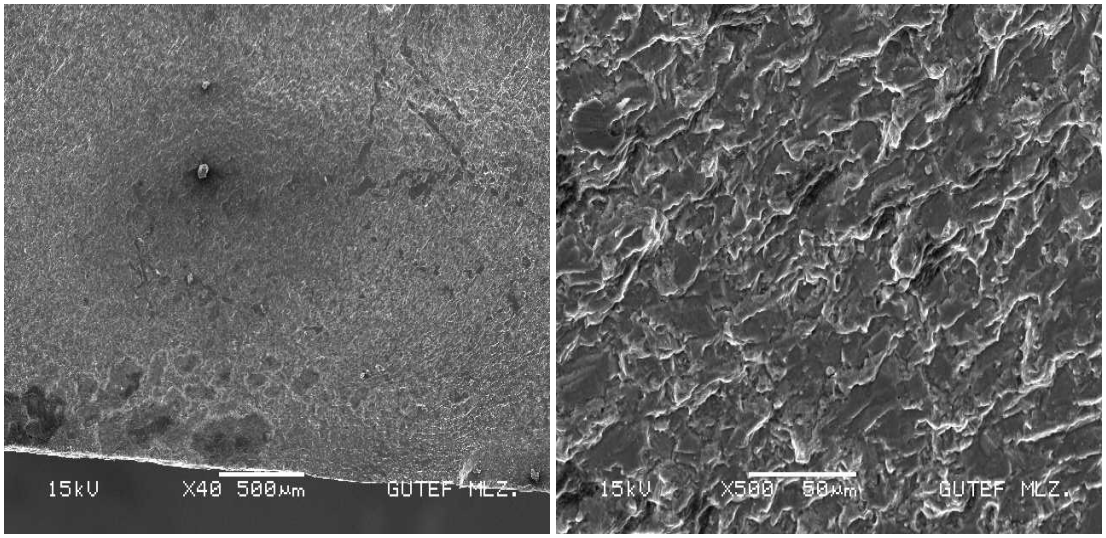
(a) (b)

Figure 4.36. SEM Views of Fracture Surfaces of 5186-H111 Side of FS Welded 5083-O/5186-H111 Joint (a:40X, 500µm-b:500X, 50µm)



(a) (b)

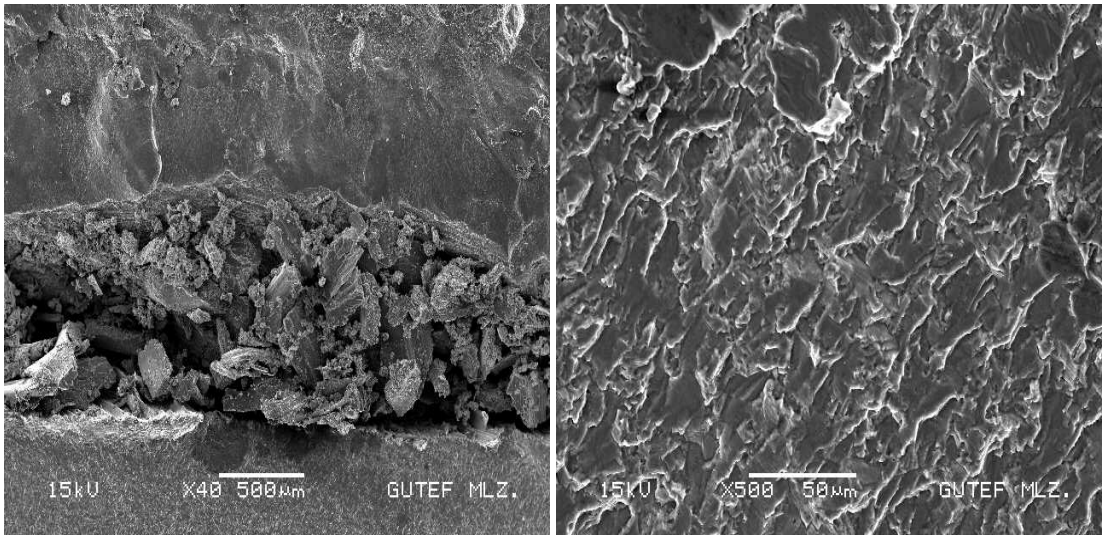
Figure 4.37. SEM Views of Fracture Surfaces of 5083-O Side of FS Welded 5083-O/5083-H111 Joint (a:40X, 500µm-b:500X, 50µm)



(a) (b)

Figure 4.38. SEM Views of Fracture Surfaces of 5083-H111 Side of FS Welded 5083-O/5083-H111 Joint (a:40X, 500µm-b:500X, 50µm)

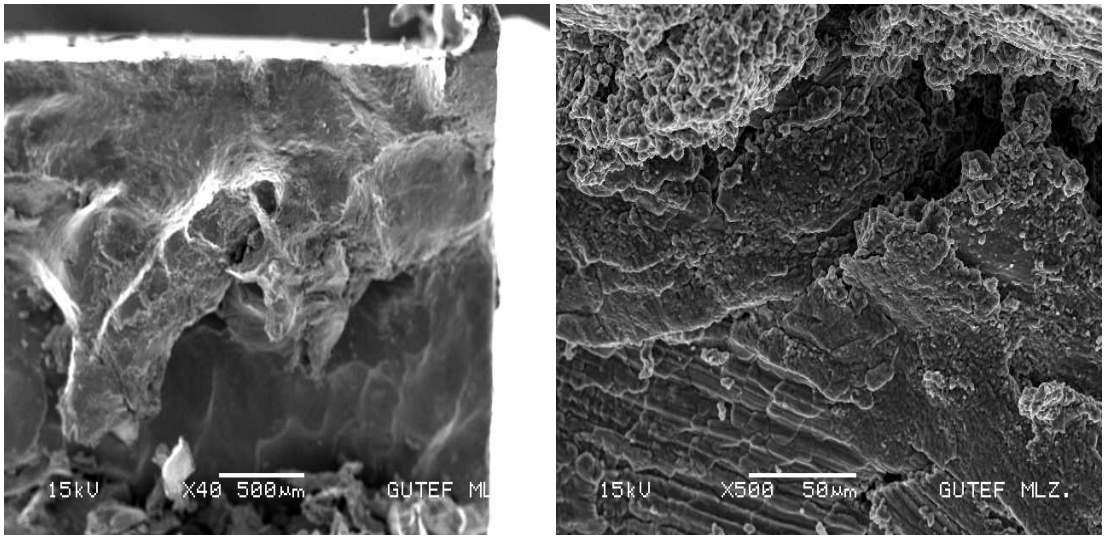
Figure 4.39.a. shows fracture surface through the fine grained nugget in a FS weld (the root to the right). Fracture is probably initiated at an imperfection in the root, or near the root in the weld/HAZ transition area due to stress intensity between fine and coarse grains.



(a) (b)

Figure 4.39. SEM Views of Fracture Surfaces of 5186-H111 Side of FS Welded 5186-H111/5083-H111 Joint (a:40X, 500µm-b:500X, 50µm)

Figure 4.40.a. and b. show the fatigue striation pattern in the area close to the root edge.



(a) (b)

Figure 4.40. SEM Views of Fracture Surfaces of 5083-H111 Side of FS Welded 5186-H111/5083-H111 Joint (a:40X, 500µm-b:500X, 50µm)

The heavily worked microstructure of the base material has been completely replaced by equiaxed grains around 10–13 µm in diameter that have little substructure, typical of a recrystallised microstructure and similar to that found previously in 5xxx, 6xxx and 7xxx series aluminium stir welds (Salem H.G., 2003) The width of the recrystallised region and its relative homogeneity, it seems likely that the microstructural changes outside the nugget are driven by the heat generated by the tool rather than the deformation induced by the tool/pin. The highly work hardened state of the parent material means that it is a highly unstable microstructure that will recrystallise readily under the high temperatures generated locally during welding.

5. CONCLUSION AND FUTURE STUDIES

5.1. Conclusion

In the present study, the similar 5186-H111/5186-H111, 5083-O/5083-O, 5083-H111/5083-H111 (Alustar) and dissimilar 5083-O/5186-H111, 5083-O/5083-H111, 5083-H111/5186-H111 aluminum alloys have been successfully joined with the FSW process using 20, 50, 80 mm/min welding speeds and 1400 rpm. Following processes have been applied.

- Sheet plates have been joined by FSW as 5083-O/5083-O, 5186-H111/5186-H111, 5083-H111/5083-H111 and 5083-O/5186-H111, 5083-O/5083-H111, 5083-H111/5186-H111, respectively.
- The tensile behavior of the 5186-H111, 5083-O, 5083-H111 base materials and the combination joints, 5083-O/5083-O, 5186-H111/5186-H111, 5083-H111/5083-H111 and 5083-O/5186-H111, 5083-O/5083-H111, 5083-H111/5186-H111 have been examined by conducting tensile tests on specimens of each type, respectively.
- The Vickers hardness tests have been conducted on the welded joints and base materials.
- Fatigue tests have been conducted in the axial loading mode, which is more severe than bending. The Woehler curves have been plotted and presented in terms of nominal stress amplitude σ_{an} and cycles to rupture N_R for joined and base specimens.
- Optical microscopy observations have been done on the FS welded 5186-H111/5186-H111, 5083-O/5083-O, 5083-H111/5083-H111 and dissimilar 5083-O/5186-H111, 5083-O/5083-H111, 5083-H111/5186-H111 on the base and near the weld zone with 10X and 40X scales.
- Scanning Electron Microscope (SEM) photographs are taken at Faculty of Technical Education at University of Gazi with Jeol JSM-6060LV Computer

Controlled Digital Scanning Electron Microscope test machine. 40X and 100X scales are used for fatigue test specimens.

The results from the obtained experimental study are bellow:

- The joint combination of 5186-H111 and 5083-O has uniform hardness distribution on HAZ. The hardness of the HAZ, in case of 50 and 80 mm/min welding speeds, is uniformly distributed and shows less variation, which ranges from 50 to 55 HV. In contrast, the hardness of the HAZ of 20 mm/min welding speed shows a very scattered value as shown in Figure 4.1. In Figure 4.2., the joint combination of 5083-O and 5083-O has uniform hardness distribution on HAZ for 20, 50 and 80 mm/min welding speeds.
- Each aluminum alloys have been successfully joined with the FSW process using 20, 50, 80 mm/min welding speeds and 1400 rpm, however FSW process should be applied up to 80 mm/min. Optional speeds of 80 mm/min welding speeds applied for better mechanical and microstructural effects.
- The variations in hardness for 5083-O and 5186-H111 joint combination are shown in Figure 4.4. The hardness of the HAZ shows more uniform values than that of the base materials due to finer and uniformly dispersed Mg_2Si particles. The solid solution hardened Al alloys showed very different behaviors of the hardness distribution in the weld zone. The hardness profile of the weld zone showed roughly homogeneous values and this was mainly governed both dislocation density and the distribution and the size of small particles.
- Stress strain curves have been plotted and compared for base materials, similar, and dissimilar joints in Figure 4.10. Table 4.1. shows the average tensile test results with each joint condition. The strengths of the HAZ of similar 5083-O FSW joint showed 281 MPa for ultimate tensile strength (UTS) and 153 MPa for yield strength (YS), which were lower strength than that of 5083-O alloy base metal. The strengths of the HAZ of similar 5186-H111 FSW joint showed 276 MPa for Ultimate Tensile Strength (UTS) and

156 MPa for Yield Strength (YS), which were approximately the same of 5083-O alloy base metal. Figure 4.7. - 4.9. show the tensile stress strain curves of FSW joints.

- The Woehler curves, presented in terms of nominal stress amplitude σ_{an} and cycles to rupture N_R, have been statically evaluated for the probabilities of 10, 50, 90 of a logarithmic Gaussian distribution.
- Sinusoidal load-time function has been used in fatigue test. The frequency was f=20 s^{-1} two stress ratios were investigated with the unnotched specimens (K_t = 1.0) under fully reversed loading ($\boldsymbol{R}= \sigma_{min}/\sigma_{max}$ = -1) using 9 specimens for the determination of each S-N curve, in Figure 4.11.-4.19. Average stresses in the interval of 60–190 MPa have been tested.
- Optical microscopy observations have been done on the each base and joint material rupture surfaces. Structure of FS welded aluminum base and joint materials are shown in Figure 4.20.-4.28. As seen in the Figures, structures are become homogenous and pore. Also grain boundaries appeared notably in Figure 4.20.b., Figure 4.21.b., Figure 4.22.b. Grain necks are constituted notably and homogeneous structure obtained, smooth and less porosity surface can be seen Figure 4.21. Shrinkage of the pores initiated with 40X in Figure 4.22.
- The FSW process have been applied on dissimilar 5083-O and 5186-H111 aluminum alloys revealed the classical formation of the elliptical ‘onion’ structure in the centre weld; this is confirmed by the microstructure with fine recrystallized grains. The Thermo-Mechanical Affected Zone (TMAZ) is also distinguished through optical microscopy. Figure 4.26.a. shows cross section of the welded specimen: particular of the nugget zone and base material interface.
- The fatigue test fracture surfaces have been examined using scanning electron microscopy. Both the weld nugget and the parent material failed in a ductile manner by the microvoid coalescence mechanism as shown in Figure 4.31.b.

and Figure 4.34.b. However, there was an absence of relatively large microvoids in the weld nugget sample and this may be a consequence of the break up of the primary constituent particles during stir welding.

- Figure 4.39.a. shows fracture surface through the fine-grained nugget in a FS weld (the root to the right). Fracture is probably initiated at an imperfection in the root, or near the root in the weld/HAZ transition area due to stress intensity between fine and coarse grains.

5.2. Recommendation of Future Studies

This study has been concentrated on the investigation in properties of welded similar and dissimilar Al alloys by Friction Stir Welding.

In future, the following considerations could be improved:

- The pin geometry could be changed.
- Different welding speeds could be applied.
- In this study, reconfigured milling machine has been used as shown in Figure 3.1. This machine could be adapted to automation.
- Friction Stir welding process may be applied to materials which are different thicknesses.
- Friction Stir welding process may be applied to more different materials. Such as brass, stainless steel etc.

REFERENCES

BENAVIDES S., LI Y., MURR L.E., BROWN D. and MCCLURE J.C., 1999, 'Low Temperature Friction Stir Welding of 2024 Aluminum', Scripta Materialia, Vol. 41, No. 8, pp. 809–815.

BOZ M., KURT A., 2004, 'The Influence of Stirrer Geometry on Bonding and Mechanical Properties in Friction Stir Welding Process', Materials and Design, 25, pp. 343-347.

CARY H.B., 1979, 'Modem Welding Technology', Prentice-Hall, Inc., Englewood Cliffs, New Jersey, pp. 223.

CAVALIERE P., NOBILER., PANELLA F.W. and SQUILLACE A., 2006, 'Mechanical and Microstructural Behaviour of 2024–7075 Aluminium Alloy Sheets Joined by Friction Stir Welding', International Journal of Machine Tools & Manufacture, 46, pp. 588-594.

CHAO B.Y.J., WANG Y. and MILLER K. W., 2001, 'Effect of Friction Stir Welding on Dynamic Properties of AA2024-T3 and AA7075-T7351', Journal of Material Processing and Manufacturing, 7(2), pp. 215-233.

CHEN C.M. and KOVACEVIC R., 2004, 'Joining of Al 6061 Alloy to AISI 1018 Steel by Combined Effects of Fusion and Solid State Welding', International Journal of Machine Tools & Manufacture.

ÇAM G., 2005, 'Sürtünme Karıştırma Kaynağı (SKK) : Al Alaşımları İçin Geliştirilmiş Yeni Bir Kaynak Teknolojisi', Makina Mühendisleri Odası Teknoloji Dünyası Dergisi, Şubat, 2005, Turkey.

DAWIS C. T. and THOMAS W. M., 1996, 'Friction Stir Process Welds Aluminum Alloys: a New Friction Welding Technique Allows Easy Welding of Normally Difficult To Join Materials', Welding Journal, 75(3), pp. 41.

DICKERSON T.L. and PRZYDATEK J., 2003, 'Fatigue of Friction Stir Welds in Aluminium Alloys That Contain Root Flaws', International Journal of Fatigue, 25, pp. 1399–1409.

DICKERSON T., SHERCLIFF H. R. and SCHMIDT H., 2003, 'A Weld Marker Technique For Flow Visualization in Friction Stir Welding', International Symposium on Friction Stir Welding.

DİLEK M., EKŞİ A.K. and BİRCAN D.A., 2006, 'The Investigation In Properties Of Welded Dissimilar Al Alloys By Friction Stir Welding', Proceedings of 11th International Materials Symposium, 19-21 April 2006, Denizli, Turkey.

EKŞİ A. and BİRCAN D.A., 2006, 'Mechanical Properties of Cold and Warm Compacted Aluminum Alloys (Al7XXX)', Proceedings of 11th International Materials Symposium, 19-21 April 2006, Denizli, Turkey.

EKŞİ A., LIPP K., SONSINO C.M., VELTL G. and, PETZOLDT F., 2006, 'Static and Fatigue Properties of The Cold and Warm Compacted Sintered Aluminium Alloy Alumix 431 (Al-5.5 Zn-2.5 Mg-1.5 Cu), Materialwissenschaft und Werkstofftechnik, Vol 37, Issue 5 , pp. 374-382.

ERICSSON M. and SANDSTROM R., 2003, 'Influence of Welding Speed on the Fatigue of Friction Stir Welds, and Comparison with MIG and TIG', International Journal of Fatigue, 25, pp. 1379–1387.

FLORES O. V., KENNEDY C., MURR L.E., BROWN D., SRİDHAR P., NOVAK B. M, and MCCLURE J.C., 1998, 'Microstructural Issues in a Friction Stir Welded Aluminum Alloys', Scripta Materialia, 38, 5, pp. 703-708.

FONDA R.W., BINGERT J.F. and COLLIGAN K.J., 2004, 'Development of Grain Structure During Friction Stir Welding', Scripta Materialia, 51, pp. 243-248.

HAAGENSEN P. J., MIDLING O. T. and RANES, M., 1995, 'Fatigue Performance of Friction Stir Butt Welds in a 6000 Series Aluminum Alloy', Proceedings of The International Conference on Computer Methods and Experimental Methods for Surface Treatment Effects II, pp. 225–237.

HANSEN M., 2003, 'A Cooler Weld', Mechanical Engineering Design.

JATA K. V., SANKARAN K. K. and RUSCHAU J. J., 2000, 'Friction Stir Welding Effects on Microstructure and Fatigue of Aluminum Alloy 7050-T7451', Metallurgical and Materials Transactions, 31A, pp. 2181–2192.

JATA K.V. and SEMIATIN S.L., 2000, 'Continuous Dynamic Recrystallization During Friction Stir Welding of High Strength Aluminum Alloys', Scripta materialia, 43, pp. 743-749.

JONHSON R. and KALLEE S., 1999, 'Friction Stir Welding', Materials World Volume 7, No.12, pp.751-753.

JUTTNER S., Fabr. 1998, Weld Met; 66:11.

LEE W.B., YEON Y.M. and JUNG S.B., 2003, 'The Improvement of Mechanical Properties of Friction-Stir-Welded A356 Al Alloy', Materials Science and Engineering, A355, pp. 154-159.

KULEKCI M. K., 2003, 'Mechanical Properties of Friction Stir-Welded Joints of AlCu4SiMg Aluminium Alloy', Kovove Materialy, 41, 2, pp. 97-105.

KULEKCI M. K. and ŞIK A., 2003, 'Sürtünme Karıştırma kaynağı ile Alüminyum Alaşımı Levhaların Birleştirilmesi ve Elde Edilen Kaynaklı Bağlantıların Özellikleri', pp. 77-86, Kocaeli, Turkey.

LEE W.B., YEON Y.M., Jung S.B., 2003, 'The Joint Properties of Dissimilar Formed Al Alloys by Friction Stir Welding According to The Fixed Location of Materials', Scripta Materialia, 49, pp. 423-428.

LIPPOLD J. C. and DITZEL P. J., 2003, 'Microstructure and Properties of Aluminum Friction Stir Welds', Materials Science Forum, pp. 426–432, pp. 4597–4602.

LIU G., MURR L.E., NIOU C.S., MCCLURE J.C. and Vega F.R., 1997, 'Microstructural Aspects of The Friction-Stir Welding of 6061-T6 Aluminum', Scripta Materialia, Vol. 37, No. 3, pp. 355-361.

LI Y., MURR L.E. and MCCLURE J.C., 1999, 'Flow Visualization and Residual Microstructures Associated with The Friction-Stir Welding of 2024 Aluminum to 6061 Aluminum', Materials Science And Engineering, A271, pp. 213-223.

MCCALL J.L. and MUELLER W.M., 1973, 'Microstructurel Analysis Tools and Techniques'.

MURR L. E., LI Y., TRILLO E. A., NOWAK B. M. and MCCLURE J. C., 1999, 'A Comparative Study of Friction Stir Welding of Aluminum Alloys', Aluminum Transactions, 1, pp. 141–154.

MURR L. E., LIU G. and MCCLURE, J. C., 1997, 'Dynamic Recrystallization in Friction Stir Welding of Aluminum Alloy 1100', Journal of Materials Science, pp. 1801-1803.

NICHOLAS E.D., 1998, 'Developments in The Friction Stir Welding of Metals', ICAA-6: 6th International Conference on Aluminum Alloys.

PEEL M., STEUWER A., PREUSS M. and WITHERS P.J., 2003, 'Microstructure, Mechanical Properties and Residual Stresses as a Function of Welding Speed in Aluminium AA5083 Friction Stir Welds', Acta Materialia, 51, pp. 4791-4801.

POLMEAR I.J. and ARNOLD E., 1995, 'Light Alloys - The Metallurgy of Light Metals', Advanced Engineering Materials, vol.1, pp. 49-51.

RHODES C.G., MAHONEY M.W., BINGEL W.H., SPURLING R.A. and BAMPTON C.C., 1997, 'Effects of Friction Stir Welding on Microstructure of 7075 Aluminum', Scripta Materialia, Vol. 36, No.1, pp. 69-75.

SALEM H. G., 2003, 'Friction Stir Weld Evolution of Dynamically Recrystallized AA 2095 Weldments', Scripta Materialia, 49, pp.1103-1110.

SATO Y. S., 2000, 'Microstructural Factors Governing Hardness in Friction-Stir Welds of Solid-Solution-Hardened Al alloys', Scripta Materialia, 43, pp. 743-749.

SATO Y. S., KOKAWA H., ENOMOTO M. and JOGAN S., 1999, 'Microstructural Evolution of 6063 During Friction Stir Welding', Metallurgical and Materials Transactions, 30A, pp. 2429–2437.

SATO Y.S., KURIHARA Y., PARK S.H.C., KOKAWA H. and TSUJI N., 2004, 'Friction Stir Welding of Ultrafine Grained Al Alloy 1100 Produced by Accumulative Roll-Bonding', Scripta Materialia, 50, pp. 57-60.

SHIGEMATSU I ., KWON Y.J., SUZUKI K., IMAI T. and SAITO N., 2003, 'Joining of 5083 and 6061 Aluminum Alloys by Friction Stir Welding', Journal Of Materials Science Letters, 22, pp. 353– 356.

ŞIK A., 2002, 'Otomobil Saçlarının MIG/MAG Kaynağında Gaz Karışımlarının Bağlantının Mekanik Özelliklerine Etkisi', Doktora Tezi Endüstriyel Teknoloji Eğitimi, Gazi Üniversitesi Fen Bilimleri Enstitüsü, Ekim 2002, Ankara, Turkey.

ŞIK A., 2004, 'MIG/MAG Metodu ile Kaynak Yapılan Yapı Çeliği (St37-2) Levhaların Eğme Yorulması Gerilmesine Çeşitli Aktif Gazlarının Etkisi', 2004 Gazi Üniversitesi Endüstriyel Sanatlar Eğitim Fakültesi Dergisi, Sayı:15, s. 45-47, Ankara, Turkey.

ŞIK A. and KAYABAŞ Ö., 2003, 'Sürtünme Kariştirma Kaynağı ile Yapilan Alüminyumun Kaynağinda Kaynak Bölgesinin Mekanik Özelliklerinin Incelenmesi', 2003Gazi Üniversitesi Endüstriyel Sanatlar Eğitim Fakültesi Dergisi Y.11, S.12, s.30-43 , Ankara, Turkey.

SUTTON M. A., YANG B., REYNOLDS A.P. and YAN J., 2004, 'Banded Microstructure in 2024-T351 and 2524-T351 Aluminum Friction Stir Welds Part II. Mechanical Characterization', Materials Science and Engineering, A364, pp. 66-74.

STARON P., KOÇAK M., WILLIAMS S. and WESCOTT A., 2004, 'Residual Stress in Friction Stir-Welded Al Sheets', Physica B, Vol 350, pp. E491-E493.

THOMAS W.M., NICHOLAS E.D., NEEDHAM J.C., TEMPLESMITH P., DAWES C.J and MURCH M.G., 1995, 'Friction Stir Butt Welding' Int Patent App PCT/GB92/02203 and GB Patent App 9125978.8, December 1991.US Patent No. 5,460,317.

THREADGILL P.L., March 1997, Bulletin, http://www.twi.co.uk/

TOTTON G.E. and MACKENZIE D.S., 2003, 'Handbook of Aluminium', vol.1.

WEISHEIT A., GALUN R. and MORDIKE B.L., 1998, 'Laser Cladding of Quasicrystal Forming Al-Cu-Fe on Aluminium', Journal of Non-Crystalline Solids, pp. 517-523.

WERT J.A., 2003, 'Microstructures of Friction Stir Weld Joints Between an Aluminium Base Metal Matrix Composite and a Monolithic Aluminium Alloy', Scripta Materialia, 49, pp. 607-612.

YASHAN D., TSANG S., JOHNS W. L., and DOUGHTY M. W., 1987, 'Inertia Friction Welding of 1100 Aluminum to Type 316 Stainless Steel', Welding Journal 66(8), pp. 27–37.

ZHOU C., YANG X. and LUAN G., 2005, 'Fatigue Properties of Friction Stir Welds in Al 5083 Alloy', Scripta Materialia, 53, pp. 1187-1191.

CURRICULUM VITAE

Murat DİLEK was born in Ordu, 1979. After being graduated from Antakya Lisesi, Hatay, he enrolled in Çukurova University, Mechanical Engineering Department of Engineering and Architecture Faculty. He graduated from Çukurova University as a Mechanical Engineer on June 2002. He started his Master of Science (MSc) education in Çukurova University Institute of Natural and Applied Sciences Mechanical Engineering Department Construction & Manufacture Division in 2002.